A Feasibility Study into Passive Online Geometric Calibration for Quadric Projection Surfaces

By

Shahid Khan
2009-NUST-MS-EE(S)-20

Supervised By

Dr. Rehan Hafiz
Assistant Professor

This thesis is submitted in partial fulfillment of the requirements for the degree of
Masters of Science in Electrical Engineering (MS EE)

School of Electrical Engineering and Computer Science,
National University of Sciences and Technology (NUST),
Islamabad, Pakistan.

Nov 2012

APPROVAL

It is certified that the contents of thesis document titled, "**A Feasibility Study into Passive Online Geometric Calibration for Quadric Projection Surfaces**" submitted by Mr. Shahid Khan have been found satisfactory for the requirement of degree.

Advisor: Dr. Rehan Hafiz

Signature: _____

Date: _____

Committee Member1:   Dr. M. Murtaza Khan

Signature: _____

Date: _____

Committee Member2:   Dr. Khawar Khurshid

Signature: _____

Date: _____

Committee Member3:   Mr. Shamyl Bin Mansoor

Signature: _____

Date: _____

To my loving family, esteemed teachers and my colleagues

CERTIFICATE OF ORIGINALITY

I declare that the research work titled **"A Feasibility Study into Passive Online Geometric Calibration for Quadric Projection Surfaces"** is my own work to the best of my knowledge. It contains no materials previously published or written by another person, nor material which to a substantial extent has been accepted for the award of any degree or diploma at SEECS or any other educational institute, except where due acknowledgment is made in the thesis. Any contribution made to the research by others, with whom I have worked at SEECS or elsewhere, is explicitly acknowledged in the thesis.

I also declare that the intellectual content of this thesis is the product of my own work, except to the extent that assistance from others in the project's design and conception or in style, presentation and linguistic is acknowledged. I also verified the originality of contents through plagiarism software.

Author's Name: <u>Shahid Khan</u>

Signature: _____

Date: _____

ACKNOWLEGMENTS

TABLE OF CONTENTS

LIST OF ABBREVIATIONS

3ds Max	3D Studio Max
FOP	Field of Projection
FOV	Field of View
MAD	Mean of Absolute Differences
MLSD	Moving Least Squares Deformation
MSE	Mean Squared Error
NCC	Normalized Cross Correlation
SAE	Sum of Absolute Errors
SIFT	Scale Invariant Feature Transform
SSIM	Structural Similarity Index Measure

LIST OF TABLES

LIST OF FIGURES

ABSTRACT

Projector-camera systems are gaining popularity in wide variety of applications like mobile phones, interactive presentations, flight simulators, games and augmented reality applications. Whenever projector is installed in a new setup, geometric calibration is performed to visually correct the projected contents. Geometric calibration techniques are classified as active online, active offline, passive online and passive offline. For applications where projection or display surface is dynamic or deformable, online geometric calibration is required to adapt the surface changes, and correct the projected imagery geometrically. This is because offline techniques cannot tackle on the fly changes of projector position or display surface. Active online techniques use imperceptible patterns along with high speed capturing cameras and Digital Light Processing projectors. These devices are expensive and imperceptible patterns reduce dynamic interval of projected contents. Passive online techniques require prior camera calibrations. Problem with prior camera calibration based solutions is that, once the relative position of projector-camera or display surface changes, camera calibration becomes void and recalibration has to be performed. This makes them unsuitable for dynamic scenarios.

In this work, feasibility study is performed and two techniques for geometric correction of 2D quadric surfaces are proposed. One technique is hybrid whereas other is passive online. Proposed hybrid technique requires offline display area estimation phase whereas passive online technique does not require prior camera calibration. In both techniques, moving least squares deformation is used to calculate the Bezier feature points. Based upon these feature points next images are prewarped using Bezier transformation. Moreover a line based metric to estimate geometric correction achieved is also introduced. After successful simulation, the algorithm is tested on real setup. It is also shown that, the work can be extended to dynamic surfaces.

INTRODUCTION

As projectors have become small, inexpensive and mobile, new user-projector interaction types are evolving. Possible user-projector interaction types are summarized in Table 1-1 [1]. Among the interaction types shown in Table 1-1, traditional surfaces are planar and viewers are sitting at single location i.e. static user, examples of such interaction are projection surfaces in class rooms and cinemas. Curved screen interactions also include static users but display environments are non planar e.g. planetarium. Planar surfaces are used in immersive workbench interactions but users may be non static e.g. virtual reality games [2]. Fourth interaction type includes non planar surfaces and non static users e.g. CAVE environment [3]. Modern interaction scenarios target the most general case of head tracked user on non planar display surfaces. Among the non planar surfaces, 2D quadric surfaces are important because applications like planetariums, immersive gaming environments and theaters demand quadric screens. The class of quadric surfaces includes ellipses, hyperbolas and parabolas. Due to such importance of these surfaces, the surfaces addressed in this work are also 2D quadric. Furthermore the geometric correction of fixed corner point dynamic surfaces (display area is deformable but corner points of display area are fixed.) is also considered. Dynamic surfaces possess the property that they can change their geometry on the fly. Using dynamic surface geometric correction methods, projectors can project on changing surfaces outdoor.

Table 1-1: Listing of user-projector interactions

Use Interaction Type / Illuminated Surface Type	Static User	Head Tracked User
Planar Display	Traditional	Immersive Workbench
Non Planar Display	Curved Screen Doom Screen	Most General Case

Whenever projectors are installed in any semi permanent or permanent setup, geometric correction (in literature words of geometric calibration and geometric correction are used interchangeably) is performed. Geometric correction refers to a group of techniques which manipulates projection system to make projected contents visually correct on projection surface. Four possible geometric calibration categories are summarized in Table 1-2 [4] and [1] .

Table 1-2: Listing of available geometric correction techniques

Calibration Method / Light Type	Online (Take input during projection, may or may not be real time)	Off-line (Adjust prior to projection)
Passive (Do not project)	Stereo, Unstructured light	Mechanical Alignment
Active (Project)	Imperceptible structured light	Laser scan, Structured light

Among the geometric correction techniques shown in Table 1-2, "passive offline techniques are mostly employed in commercial applications" [4]. These techniques use precise electro-mechanical alignment tools to register the projected contents on planar display surfaces, such as perpendicular projection on planar surface from known distance [4]. These techniques do not work if the projection surfaces are non planar. Active offline techniques use predefined patterns to estimate surface. These techniques fail to correct on the fly changes, because these techniques are intrusive and interrupt normal projection during calibration. Active online techniques use imperceptible patterns and Digital Light Processing projector. Such techniques reduce dynamic interval of projected contents because imperceptible patterns use bit planes of projected imagery. Passive online techniques use prior camera calibrations.

1.1 Motivation

Recent developments in projector based applications have heightened the need for passive online geometric correction (geometric distortion correction is a fundamental issue of projector based

applications [5]). A huge body of literature about geometric correction exists, however a few

techniques of passive online geometric calibration are available [4], [5], [6], [7], [8], [9] and

[10]. In existing techniques either prior camera calibration (all systems which perform automatic

geometric correction use cameras to sense the projection environment.) is required or

computation time is too high. Camera calibration is a process in which camera parameters and

camera-projector relationships are determined. The problem with camera calibration based

solutions is that whenever mutual position of camera and projector changes, a new calibration

phase must be initiated to re-estimate the subject relation. Therefore a technique based upon

passive online geometric calibration is required which can perform calibration without prior

information. Applications which include dynamic surfaces and non static users will be

beneficiaries of such technique.

1.2 Problem Statement

To devise a passive online geometric correction scheme that avoids camera calibration.
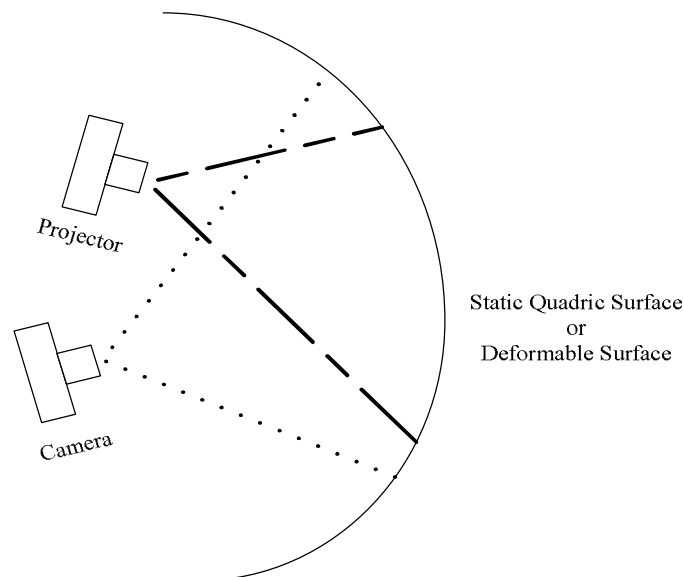
Figure 1-1: Projection setup

The setup of projection system being considered is shown in Figure 1-1. The setup includes one

camera projector pair and a projection surface. The projection surface is quadric and may be static or deformable in case to case basis.

1.3 Contributions

Contributions of this work are:

1. Proposed a hybrid approach based upon active offline display area estimation (localization of projected contents in captured image) and passive online geometric correction phases.

2. Proposed a passive online geometric calibration technique using Moving Least Square Deformation [11] along with Bezier transformation [12] and [13] without offline display area estimation phase.

3. Devised a line based error metric to quantify amount of geometric correction.

1.4 Thesis Organization

Thesis is organized in five chapters. Literature review of the available geometric calibration categories is given in Chapter 2. Methodology and results of the proposed techniques regarding geometric correction are described in Chapter 3. The findings of this work are summarized in Chapter 4. The thesis is concluded in Chapter 5, with proposals of some possible extensions to this work.

LITERATURE SURVEY

A considerable amount of literature has been published on geometric correction of projection systems. The algorithms proposed in published literature can be divided in five main categories. This chapter is composed of five parts and each part present literature review of one geometric correction category.

2.1. Passive Offline Techniques

2.2. Active Offline Techniques

2.3. Active Online Techniques

2.4. Passive Online Techniques

2.5. Hybrid Techniques

2.1 Passive Offline Techniques

Such techniques used electromechanical systems like motors or manual adjustment levers. Generally in controlled environment, key stone correction and perspective correction of images on perpendicular projection optimized surfaces was required. For example whenever a projector is installed in class room, such manual adjustments are done to show the visually correct image on the display surface. These techniques used time consuming procedures along with cumbersome alignment techniques for geometric calibration [1] and [4]. Since these techniques could not prewarp the projected contents therefore these techniques cannot be used for non planar surfaces.

2.2 Active Offline Techniques

In such techniques, known visible patterns were projected and warping functions were calculated

based upon corresponding captured pattern images. These warping functions were then used to prewarp next projected images for the sake of geometric correction. Common processing steps of these techniques are given in Figure 2-1.

```
┌─────────────────────────────────────────────┐
│            Project pattern image             │
└─────────────────────────────────────────────┘
                       │
                       ▼
┌─────────────────────────────────────────────┐
│        Capture projected pattern image       │
└─────────────────────────────────────────────┘
                       │
                       ▼
┌─────────────────────────────────────────────┐
│      Find projected pattern in captured image │
└─────────────────────────────────────────────┘
                       │
                       ▼
┌─────────────────────────────────────────────┐
│   Establish correspondence between projected and │
│          captured pattern points             │
└─────────────────────────────────────────────┘
                       │
                       ▼
┌─────────────────────────────────────────────┐
│   Calculate warping function based upon established │
│                correspondence                │
└─────────────────────────────────────────────┘
                       │
                       ▼
┌─────────────────────────────────────────────┐
│  Generate lookup table and start projection of actual │
│  contents after warping using calculated lookup table │
└─────────────────────────────────────────────┘
```
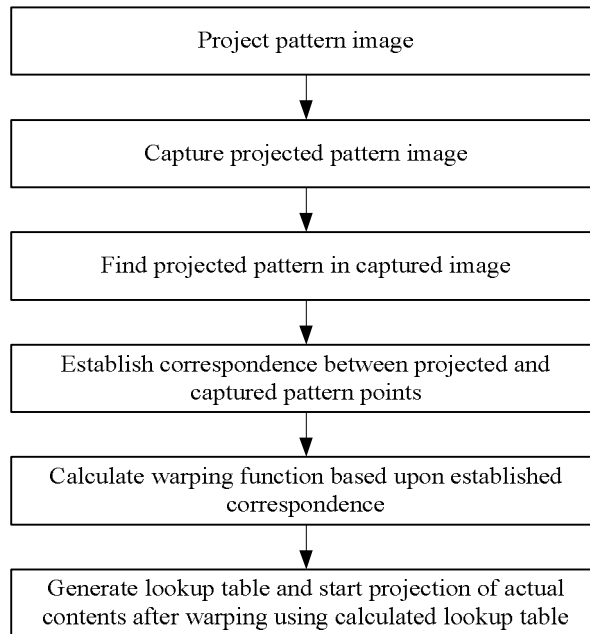
Figure 2-1: Processing steps for active offline geometric correction

Several successful attempts had been done in this category [14], [15], [16], [17], [18], [19] and [20]. Among the proposed techniques, laser and physical fiducials based techniques were intrusive and therefore annoying to the user. Offline pattern based techniques could not tackle the problem of runtime surface or system misalignment, because once any misalignment occurs in the system, normal projection must be stopped to perform recalibration of the system.

Atif et al. [12] proposed an approach of active offline geometric calibration. In the proposed work, structured pattern was used to compute a lookup table. Based upon this lookup table, subsequent images were warped using Bezier transformation.

2.3 Active Online Techniques

Mainly two approaches were deployed in such techniques. First was based upon fast camera

rendering and second was imperceptible pattern based. Raskar et al. [21] and Cotting et al. [22] proposed their approaches using DLP (Digital Light Processing) projectors. Imperceptible patterns could be embedded by turning on and off every pixel of DLP projectors because in these projectors every pixel was generated by micro mirrors tilting towards the screen. In the reported solutions high speed cameras were used to capture the images. Since patterns were projected at very high speed, human eyes could not perceive the patterns however camera could see the actual pattern and based upon these patterns geometry of the surface was estimated.

Imperceptible patterns based surface estimation was done in [23], [24] and [25]. In the proposed algorithms, light of projected contents was varied using predefined algorithms to embed the codes. Upon capturing the image, codes embedded using light variations were extracted. In demonstrated methods so far, both spatial and temporal modulation schemes had been utilized. The problem with active online techniques was reduction in available dynamic interval of the projected imagery because they used bit planes of actual projected contents. The algorithms, which used DLP projectors also reduced dynamic interval of these projectors [5].

Park et al. [8] worked for dynamic surfaces and presented technique using imperceptible pattern. In the proposed algorithm spatial encoding was used and work for radiometric and geometric corrections of dynamic surfaces was presented. Like other active online geometric calibration techniques, display quality of the projection was poor due to reduction of available dynamic interval of projected imagery.

2.4 Passive Online Techniques

Two categories of approaches had been proposed. The approaches of first category employed stereo camera based algorithms. In stereo algorithms prior camera calibrations were required. Moreover "if correlation based methods are used to establish correspondence between projected

and captured image pairs, results are unreliable" [4]. So these algorithms could not be used for geometric calibration of dynamic surfaces. The approaches of second category used unstructured video (actual projected contents) to perform geometric correction. These methods used initial camera calibrations and assumption of fixed camera projector relative position [4], [9], [5] and [10]. The passive online technique proposed in this thesis also belongs to this category. Following are some of the published passive online techniques.

Yang and Welch [4] proposed an approach of passive online calibration technique. In the proposed technique, stochastic frame work was used to update the display surface estimate. The algorithm started with known camera projector relationship and a crude estimate of the surface. Correlation based matching between camera and projected image pair was found along the epipolar lines. This matching was done for a selected subset of features permuted from a set of projected features. In this way 3D surface estimate was acquired and updated per frame. Accuracy shown in the results was calculated after 45 min continuous running of the system. For complex surfaces, denser grid of features would be required and the proposed system would take even longer time. Since this technique starts with known relationship between camera and projector, moreover results demonstrated are for static surfaces.

Choi et al. [7] presented an approach without using any warping. The function used to perform the correction was based upon degree angle of a mirror placed in front of the projector. The experimentation setup consisted of a parallelepiped room with compensated projector movements. Reported frame rate was 27.3fps however the work was limited to planar surfaces.

Yamanaka et al. [9] presented an approach for dynamic projector case in which prior camera calibration was performed. 2D dynamic programming along epipolar lines was used to find the correspondence between projected and captured images. Based upon these correspondences B-

splines were computed to prewarp the next image. The work was for non planar surfaces.

Drouin et al. [5] and [10] used unstructured video for the geometric calibration. In the identified algorithm, a gray level quanta was assigned to each pixel. The 3D shape of the scene was then reconstructed using quanta motion detected from the captured and projected image pair. The limitation of the work was fixed relative position of projector-camera pair. Moreover the work was presented for piecewise planar surfaces.

2.5 Hybrid Techniques

Zollman et al. [26] proposed a hybrid technique. In the reported work, virtual canvas (a structured light pattern) was shown initially to estimate the display area of the surface. Then a fast point pattern (a grid of points where each point could be turned on and off representing binary one or zero) was projected and projector-camera pixel correspondence was calculated. Based upon this correspondence, a lookup table was generated. Subsequent images were warped using this lookup table. The calculated look up table had warping values for the points where projected pattern was displayed. To generate warping values for the rest of the image areas, trilinear interpolation was used. After this offline phase, optical flow was used to calculate next camera projector approximation. However this procedure was only warranted to work for small camera-projector movements, because "optical flow is not reliable beyond certain level of movement. Once movement becomes large, a new phase of offline calibration is started and new warping lookup table is calculated". This technique was of little use because it did not warrant the online geometric correction after certain level of geometric distortion.

Fuchs et al. [6] proposed predictive rendering to get the predicted image and then based upon this image actual features of the projected and captured images were matched. Based upon feature matches, the pose of projector was estimated. Successful implementation for moving

projector was demonstrated. Initial camera calibration was required in this technique.

Zhou et al. [27] also proposed a hybrid technique. Basic display unit was a projector with sensors, computation and networking capability. A camera was attached to each projector and in offline phase camera was calibrated using structured light pattern (a predesigned pattern), while in the second phase an online check for the changes in projected contents was performed. This technique again used camera calibration.

<div align="center">

Table 2-1: Literature review summary

</div>

Approach	Type	Require camera calibration	How it calculate warps	How it monitor for change	Applicable surface	Can work for dynamic surfaces
Yang & Welch 2001[4]	Passive	Fixed camera projector position	Feature matching	Correlation	Planar, curved	May be after computational optimization
Yamanaka 2010 [9]	Passive	Yes	B spline surface	Along epipolar lines	Non planar	
Drouin 2011 [5] Drouin 2010[10]	Passive	Fixed camera projector position	Estimated 3d surface	Matches activity pattern	Piece wise planar	Yes, but for piece wise planar surfaces only
Cotting 2005 [22]	Active	Yes	Pixel level alpha mask	Imperceptible patterns	Arbitrary surface	Yes, but with reduced dynamic interval
Zollman 2007 [26]	Hybrid	Yes	Structured light pattern	Optical flow	Planar	No
Jonson & Fuchs 2007 [6]	Hybrid	Yes	Structured light pattern	Feature matching	Complex, Room Corners	Maybe
Zhou 2008 [27]	Hybrid	Yes	Structured light pattern	Camera per projector, Normalized cross correlation	Planar	Yes, but for planar surfaces only
Atif 2011 [12]	Active	No	Bezier	Do not monitor	Quadric	No
Proposed	Hybrid	Yes	MLSD, Bezier transformation	MLSD	Quadric	Yes
	Passive	No				

The summary of techniques surveyed is presented in Table 2-1. Among the techniques shown in Table 2-1, if Yang [4] and Yamanaka [9] are computationally optimized, their use may be extended to the scenarios where surfaces are dynamic (including planar and quadric changes) and projector-camera relative positions are fixed. This is because, algorithms proposed in [4] and

[9] had a fundamental constraint of fixed camera-projector relative position. This fix relative position constraint is due to initial camera calibration. Unlike [4] and [9], a technique is desired which could be extended to the scenarios where camera projector relative position is changing (without camera calibration). The technique proposed in this work does not require prior camera calibration. Therefore if proposed passive online technique is computationally optimized and moving corner points are estimated at run time. It may be extended to the scenarios where surfaces are dynamic and projector-camera relative position is changing.

<div align="right">

Chapter 3

</div>

<div align="center">

GEOMETRIC CALIBRATION

</div>

In this chapter methodology to achieve the task of geometric correction and results obtained are presented. First, all the terminologies used are discussed and then proposed distortion estimation metric is presented, at the end of this chapter methodology and results are discussed.

3.1 Terminology

Terminologies used in this chapter are as follows.

3.1.1 Projector Domain Image

The image projected via projector is called projector domain image $\{I_{PD}\}$. Projector domain image $\{I_{PD}\}$ is illustrated in Figure 3-1(a).

3.1.2 Camera Domain Image

When the projector domain image $\{I_{PD}\}$ is projected on a surface and is captured by a camera, it is termed as camera domain image $\{I_{CD}\}$. Camera domain image is shown in Figure 3-1(b).

<div align="center">

(a)   (b)   (c)

Figure 3-1: Images of projector domain to camera domain conversion process
(a) Projector domain image, (b) Camera domain image, (c) Domain converted captured image

</div>

3.1.3 Conversion from Camera Domain to Projector Domain

For correspondence estimation between camera domain image $\{I_{CD}\}$ and projector domain image $\{I_{PD}\}$, both images should be in same domain. Domain conversion is the process in which camera domain image $\{I_{CD}\}$ is transformed from camera domain $\{CD\}$ to projector domain

$\{PD\}$, symbolically $\{CD \, ? \, {}^{DomainConversion} \, ? \, ? \, ? \, ? \, ? \, ?? \, PD\}$. The image obtained from domain conversion shall be termed as domain converted captured image $\{I_{DC}\}$. Domain converted captured image is provided in Figure 3-1(c).

3.1.4 Line Images

To estimate frame distortion, separate images containing vertical and horizontal lines are projected, these images shall be termed as horizontal line image and vertical line image respectively. Both images are shown in Figure 3-2. The details on manipulation of these images for geometric distortion calculation are given in section 3.4. The projected lines used in this work were 2 pixels (thickness was selected arbitrarily based upon resolution of the image) thick whereas thickness of lines in captured images depends on the resolution of captured images.

(a)   (b)
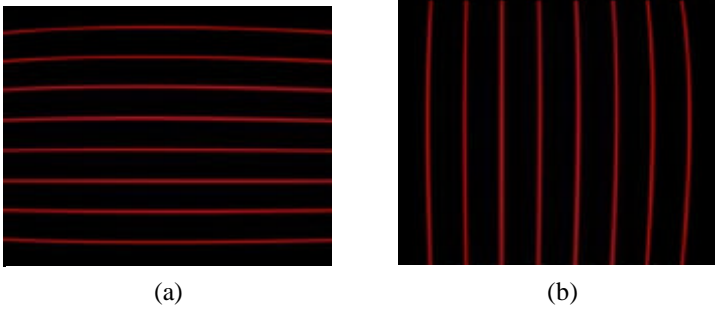
Figure 3-2: Line images for distortion estimation algorithm
(a) Horizontal line image, (b) Vertical line image

3.1.5 Background Image

An image without any contents is projected and captured, to eliminate ambient lighting effects from the subsequent captured images. This image is kept as background image $\{I_B\}$ and all captured images are subtracted from this image before any processing i.e. $(I_{CD} \, ? \, I_B) \, ? \, {}^{I_B} \, ?? \, I_{DC}$.

3.1.6 Homography

Homography $\{H\}$ is a 3x3 matrix, used to perform geometric transformations on the image. Other names of homography are projective and similarity transform, it allows 8 degree of

freedom and preserves straight lines [28]. Homography has been used for geometric correction of projection systems on planar surfaces [19]. It is a linear operation used to perform geometric corrections e.g. keystone correction. In this work homography is used to convert images from camera domain to projector domain { I_{CD} ? $\overset{H}{?}$? I_{DC} }. Justification for the use of homography is that, since homography is a linear operation, it preserves all the nonlinearities of the camera domain image { I_{CD} } while converting it to domain converted captured image { I_{DC} }. The nonlinear geometric relationships can thus be reliably extracted in the subsequent steps.

3.1.7 Bezier transformation

Bezier transformation { BT } is an nth degree polynomial parametric transformation [13], which requires set of control points to prewarp (projected image is warped to prevent geometric distortion in domain converted captured image) the image. Details of Bezier transformation { BT } and Bezier subdivision { BSD } are given in appendix A. In this work 2nd order Bezier transformation { BT } along with 0th level Bezier subdivision { BSD } is used to perform the transformations, because surfaces used are purely quadric.

3.1.8 Bezier Feature Point

Locations of Bezier control points { B_{CP} } as detailed in appendix A are predefined. When an image is projected, SIFT [29] features of the image corresponding to Bezier control points { B_{CP} } shall be termed as Bezier feature points { B_{FP} }. The Bezier feature points { B_{FP} } of projected image { I_{PD} } shall be referred as projected Bezier feature points { B_{PFP} }.

3.1.9 Moving Least Squares Deformation

Moving Least Squares Deformation { $MLSD$ } [11] warps the provided grid of points using pre established correspondence between image pairs. Correspondence is in terms of points or lines termed as handles in [11]. After establishing the correspondence between image pair, rigid,

affine or similarity transformation can be used to perform the warping [11]. In this work, point based correspondence and similarity transformation are used. Since transformations used by MLSD are linear so Bezier feature point calculation process has an implicit assumption of planar projection surface. However this assumption is again justified (homography is also linear as discussed in section 3.1.6) because nonlinearities of the surface are catered in subsequent Bezier transformation phase. Moreover in this work, SIFT [29] is used to establish correspondence between projector domain image and domain converted captured image pair. Based upon this correspondence, MLSD [11] computes and applies the warping on provided grid of 3x3 points. The resulting warped grid shall be termed as captured Bezier feature points $\{B_{CFP}\}$. MATLAB Implementation of MLSD is available from [30].

3.1.10 Exhaustive Search

Block based matching {BBM} algorithms use blocks in the images to find matches between image pairs. Exhaustive search is an algorithm of block based matching. Different terms for exhaustive search are as followed.

? Search algorithm is the pattern, in which block based match is sought in the image.

? Block size is the size of image used for cost function calculation.

? Search window is the area of image, in which block based match is searched.

? Cost function is matching criterion based upon similarity or difference. In search window at specific points, defined according to search algorithm, cost function is computed.

The motion estimation algorithms require description of search algorithm, search window, cost function and block size (8x8, 16x16 etc) to calculate the match between two image segments. The search algorithm used in this work is exhaustive search (it is a brute force method which tries to find the match at all possible locations in search window). This search algorithm was

selected because focus of current work was to check the feasibility of block based techniques for passive online geometric correction. The points corresponding to Bezier control points $\{B_{CP}\}$ at which exhaustive search pattern based matching was done are shown in Figure 3-3(a). The definitions of search window and block size are shown in Figure 3-3(b).

(a)   (b)
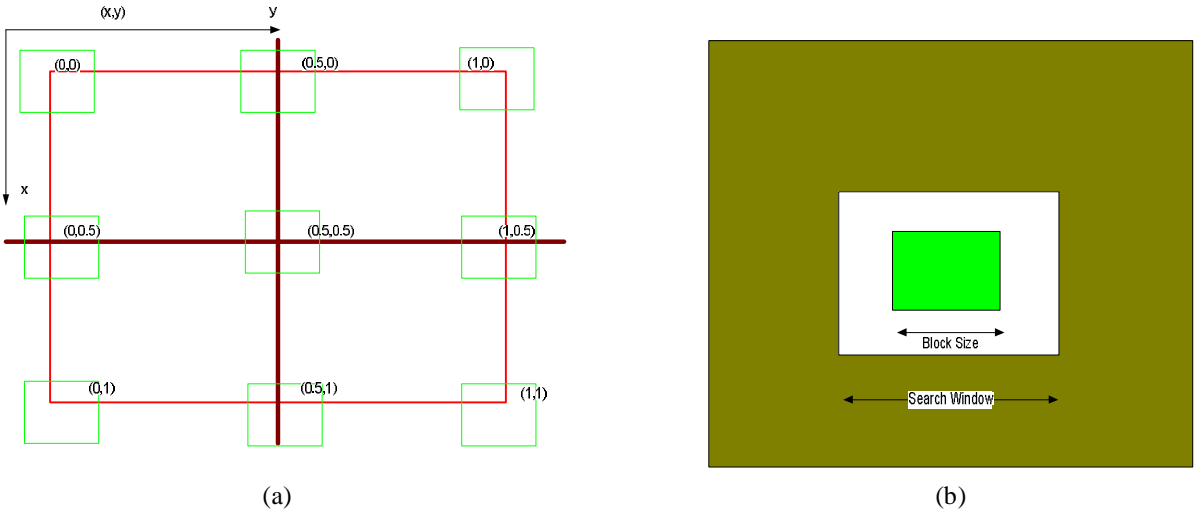
Figure 3-3: Block based matching
(a) Search pattern used on the image, (b) Full search pattern

3.1.11 Feature Extraction.

Features extraction is the process through which, strong descriptors from the images are extracted. Later on these features are used to find correspondence between image pairs. In this work, Scale Invariant Feature Transform {SIFT} [29] is used to find and match the feature descriptors in the image pair.

3.2 Test Environment

To verify the proposed approach of geometric correction, two test environments were deployed.

1. A 3ds Max based simulation frame work.

2. A physical setup using quadric surface (Curved dome).

In this section test environment of both simulation and experimental setups is described.

Moreover simulation of dynamic surfaces is also described. Setup used to validate the proposed approach consists of a projection surface, projector and a camera as shown in Figure 3-4. Projector is used to project projector domain image $\{I_{PD}\}$ and camera is used to acquire camera domain image $\{I_{CD}\}$.
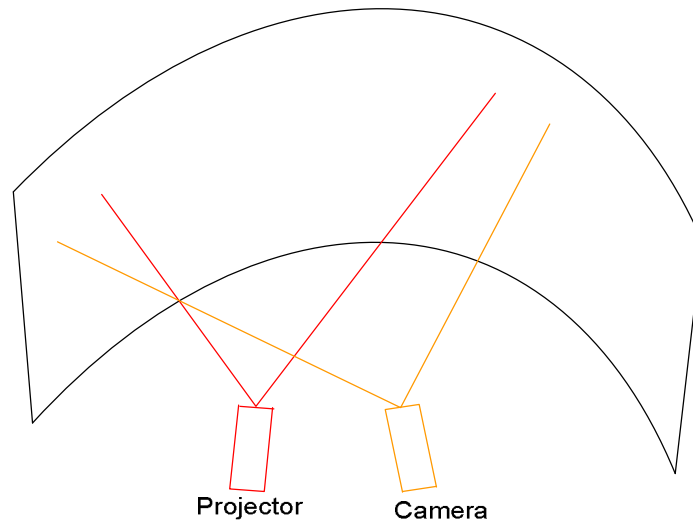
Figure 3-4: Test setup

3.2.1 Simulation using 3ds Max: Curved Surface

Since experimentation setup should be able to project the image on projection surface and capture the displayed contents, simulation setup should also exhibit both of these characteristics. Both 3ds Max and MATLAB were used for the simulation. MATLAB was the core programming platform and 3ds Max was used to generate different types of projection surfaces, camera and projector.

Max script was used to write a rendering script and this script was used to communicate with the 3ds Max. The GUI of 3ds Max is provided in Figure 3-5. File handling based approach was used to perform the operations. MATLAB saved prewarped image into a file and then invoked 3ds Max to apply surface deformation on the image. Output of 3ds Max was saved in a file again.

Subsequently this file was read by MATLAB and distortion estimation metric or correspondence estimation procedure, as appropriate was applied on the image.
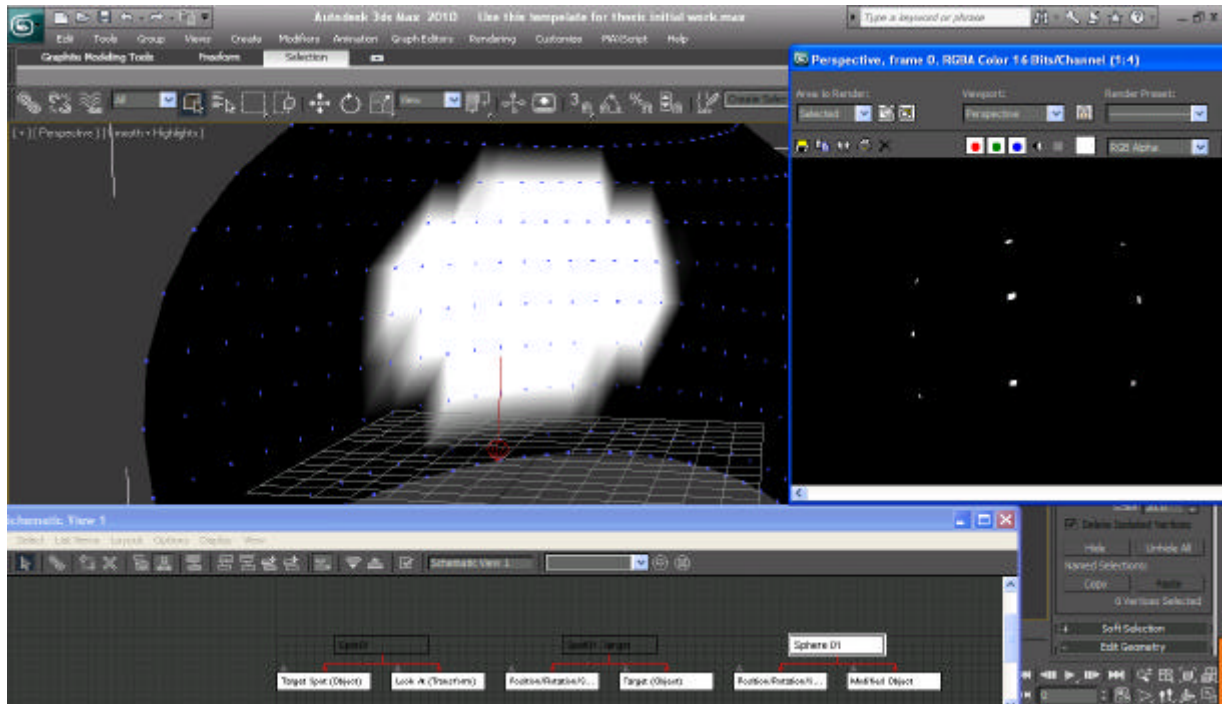
Figure 3-5: Simulation setup for the implementation

3.2.2 Practical Testing Environment: Curved Dome

To perform practical test, projector NEC M420x and a digital camera Cannon 450-D were used. Since the focus of the work was to check the feasibility of technique, MATLAB was used as the prototyping platform. The only constraint on the setup is that, field of view of camera must contain the complete field of projection of projector because computer based algorithm can process only those parts of the surface which camera can see. The layout of camera and projector used for experimentation are shown in Figure 3-4.

3.2.3 Simulation using 3ds Max: Dynamic Surface

3ds Max was used to simulate the fixed corner point dynamic surface (only display area was deformable whereas corner points of display area were fixed), since dynamic/deformable surfaces can change their geometry while actual contents are being displayed on the screen e.g.

an outdoor projection surface. To simulate the dynamic surface effect, several planar and quadric surfaces were designed in 3ds Max and after certain number (3 frames in this work) of frames surface was changed to simulate the effect of dynamic surface. The algorithm of dynamic surface simulation is shown in Figure 3-6.
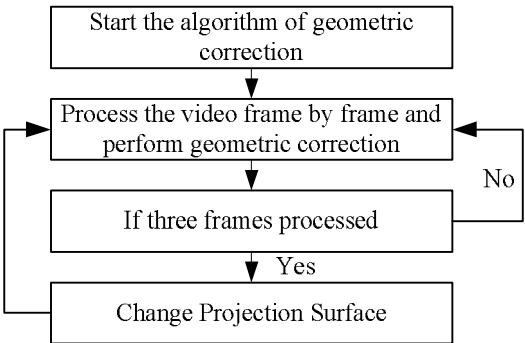
Figure 3-6: Algorithm to simulate dynamic surfaces

3.3 Test Sequences

Four video sequences illustrated in Figure 3-7 were used for testing. The resolution of all the video sequences was 352x288 in YUV 420 format. They had been downloaded from [31]. Instead of using individual images in YUV, color space conversion from YUV to RGB format was performed and these RGB images were saved as mat file. Moreover for practical experimentation, four wallpapers of resolution 1024x768 were used [32]. These images are illustrated in Figure 3-8.

(a)   (b)   (c)   (d)
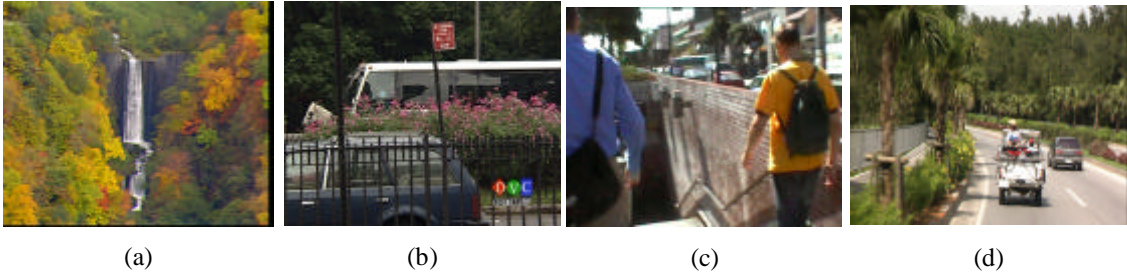
Figure 3-7: Test sequences for the simulation based testing
(a) Waterfall sequence, (b) Bus sequence, (c) Walk sequence, (d) Driving sequence
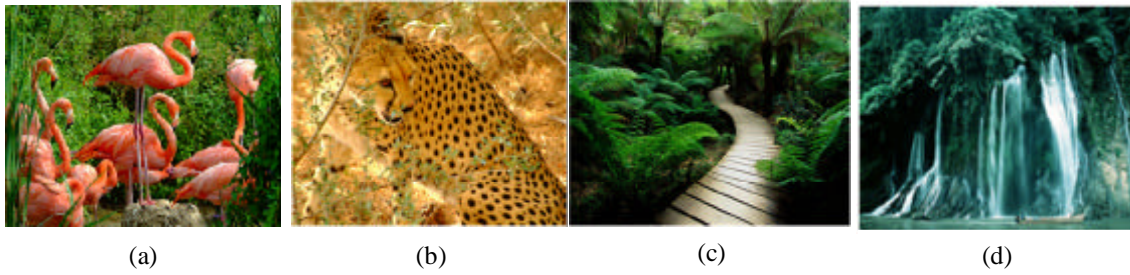
Figure 3-8: Test images used for practical testing
(a) Image 1, (b) image 2, (c) image 3, (d) image 4

3.4 Proposed Distortion Estimation Metric

In order to quantify amount of geometric distortion (or geometric correction alternatively) in captured images, line based geometric distortion estimation metric (metric is termed as line based because it uses the line images discussed in section 3.1.4) is introduced in this work. This metric is defined using Figure 3-9, Equation 3-1 and Equation 3-2. As apparent from the definition, the line based distortion estimation metric is normalized sum of Euclidian distances between captured curved lines and estimated straight lines.
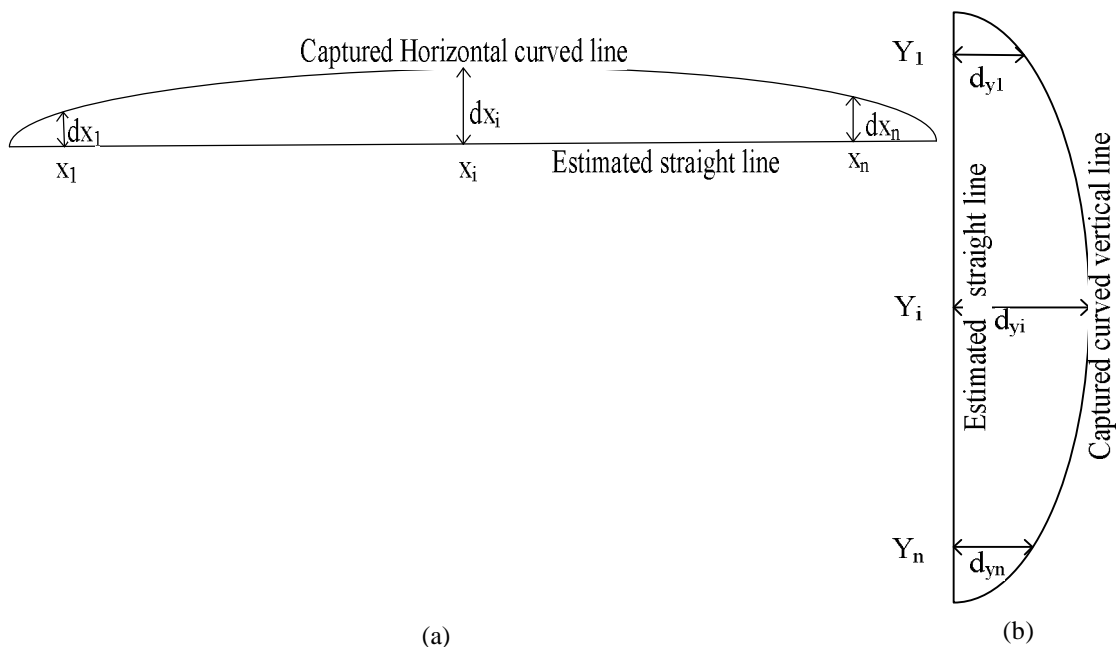
Figure 3-9: Distortion estimation metric for detected lines
(a) Horizontal line, (b) Vertical line

20

$$HorizontalLineDistortion(D_H) \approx \frac{\sum_{i=1}^{n} d_{xi}}{|x_n - x_1|} \quad \textbf{Equation 3-1}$$

Where d_{xi} is the Euclidian distance in terms of pixels between curved line and estimated straight line at x_i^{th} point

$$VerticalLineDistortion(D_V) \approx \frac{\sum_{i=1}^{n} d_{yi}}{|y_n - y_1|} \quad \textbf{Equation 3-2}$$

Where d_{yi} is the Euclidian distance in terms of pixels between curved line and estimated straight line at y_i^{th} point

These line distortions were calculated for every vertical or horizontal line of the captured image (separate horizontal or vertical line images as given in section 3.1.4, were projected for horizontal or vertical distortion estimation respectively). Then complete distortion estimate of horizontal or vertical direction was obtained by averaging the metric values obtained for each horizontal or vertical line respectively. Equation 3-3 and Equation 3-4 give method of calculating total image distortion in horizontal or vertical direction respectively.

$$HorizontalDistortion \approx \frac{\sum_{i=1}^{N} D_{H_i}}{N} \quad \textbf{Equation 3-3}$$

$$VerticalDistortion \approx \frac{\sum_{i=1}^{N} D_{V_i}}{N} \quad \textbf{Equation 3-4}$$

Where

? N is number of detected lines.

? Horizontal distortion is the distortion estimated from the horizontal lines captured image.

? Vertical distortion is the distortion estimated from the vertical lines captured image.

The algorithm of achieving distortion estimate using line image is as followed.

Algorithm: Line Based Image Distortion Calculation

Input: Background image, line captured image

1. Subtract line captured image from background image.

2. Convert subtracted image from RGB to gray scale.

3. Dilate gray scale image and convert it to binary image (skip dilation step if captured lines have appropriate width to yield continuous edges).

4. Apply Canny edge detector on binary converted image.

5. Crop the edge detected image from right, left, top and bottom by 20 pixels.

6. Use edge linking on cropped image to detect the lines.

7. For each detected line

    i. Define a straight line approximation.

    ii. Find absolute point to point Euclidian distance between estimated straight line and detected curved line.

    iii. Sum up all the Euclidian distances.

    iv. Divide the resultant sum by length of the estimated straight line for normalization.

8. Average all resultant sums obtained in step 7.

Output: Frame distortion

Images from intermediate steps of line based frame distortion calculation algorithm for horizontal line image are shown in Figure 3-10. Background image is illustrated in Figure 3-10(a). This image is subtracted from subsequent frames to eliminate ambient lighting effects. Captured image corresponding to horizontal projected lines is presented in Figure 3-10(b). RGB captured image is converted to gray scale for edge detection as shown in Figure 3-10(c). This gray scale image is dilated (dilation is performed in this particular case to eliminate the

discontinuity in the lines because at some areas lines were broken. It may not be necessary where camera domain images have continuous lines) and then converted to binary image. The binary converted image is illustrated in Figure 3-10(d) and then Canny edge detector is used to extract the edges. The output of Canny edge detector is shown in Figure 3-10(e). Output of Canny edge detector is cropped form left, right, top and bottom as shown in Figure 3-10(f). The sides are cropped to separate the ends of detected lines which are connected together because these connected ends were giving false impression of continuous line to edge linking algorithm. Edge linked image is shown in Figure 3-10(g). As apparent from the Figure 3-10(g), output of canny edge detector gives dual edges for each line (both edges were considered, because it did not make any change in results due to normalization and averaging). Based upon output of edge linking algorithm, straight lines for each detected captured curved line were estimated and then using Equation 3-1 and Equation 3-3, values representing horizontal distortion were calculated.

Since final outputs were numeric values representing horizontal and vertical distortions for particular frame. These distortions were then plotted against frame numbers i.e. for every processed frame number corresponding horizontal or vertical distortion was plotted along vertical line and corresponding frame number was plotted along horizontal line. In this way two graphs, one representing horizontal distortion profile and other representing vertical distortion profile were obtained for each processed sequence. One of such plots, representing horizontal geometric distortion profile is shown in Figure 3-10(h).

It is apparent from Figure 3-10(h) that, 32 frames of the video sequence were processed by the algorithm. The maximum horizontal geometric distortion of 1.8 occurred at 1st frame and minimum horizontal distortion occurred at 10th frame i.e. 0.4. Whereas maximum horizontal distortion after 1st frame was observed at 20th frame, value of this distortion was 1.0. In this

manner whole behavior of geometric correction algorithm can be observed from plotted distortion profiles.

(a)　　　　　　　　(b)　　　　　　　　(c)　　　　　　　　(d)

(e)　　　　　　　　(f)　　　　　　　　(g)　　　　　　　　(h)
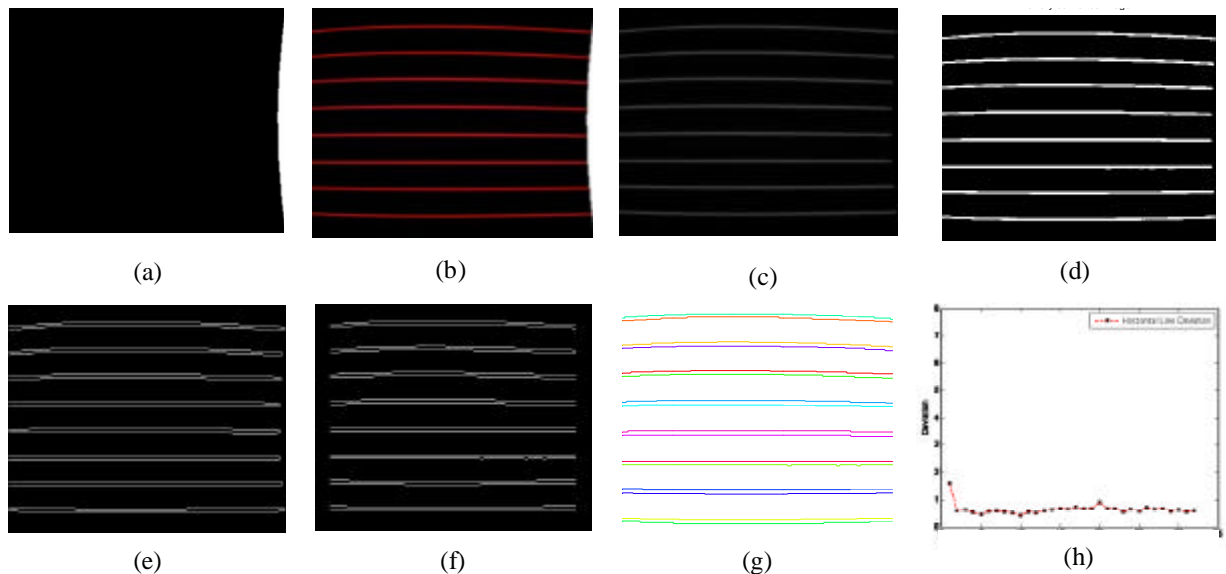
Figure 3-10: Intermediate steps of line based distortion estimation metric
(a) Background Image, (b) Projected Image, (c) Gray Scale image (d) Dilated and binary converted image, (e) Edge extracted, (f) Sides cropped, (g) Edges Linked, (h) Horizontal distortion profile

Using the proposed metric, a new figure of merit (reflecting achieved geometric correction in the image) termed as cumulative % age of correction achieved {CC%} was also calculated. The formula of *CC%* calculation is given in Equation 3-5.

$$CC\% \ ? \ (1 ? \frac{\frac{ReducedHorizontalDistortion}{InitialHorizontalDistortion} ? \frac{ReducedVerticalDistortion}{InitialVerticalDistortion}}{2}) * 100 \quad \textbf{Equation 3-5}$$

Where

? *CC%* is cumulative % age of correction achieved

? Initial Horizontal Distortion {IHD} and Initial Vertical distortion {IVD} are calculated from captured image before application of geometric correction algorithm

? Reduced Horizontal Distortion {RHD} and Reduced Vertical Distortion {RVD} are calculated from captured image after application of geometric correction algorithm

Formula of Equation 3-5 is opted because it represents the amount of cumulative correction

achieved linearly from 0% (no geometric correction) to 100% (full geometric correction). Interpretation of CC% values is provided in Table 3-1.

Table 3-1: Interpretation of CC% values

Test case	Initial horizontal distortion	Reduced horizontal distortion	Initial vertical distortion	Reduced vertical distortion	CC%
Case 1	1	1	1	1	0
Case 2	1	0	1	0	100
Case 3	1	1.3	1	1.3	-30
Case 4	1	2	1	2	-200

In the Table 3-1, case 1 shows the case of no geometric correction i.e. RHD and RVD are equal to IHD and IVD respectively. Whereas case 2 of Table 3-1 highlights the event of full geometric correction i.e. there is no RHD and RVD left in camera domain images. Negative values of CC% indicate that geometric distortion is induced in the resultant images instead of geometric correction. Case 3 and Case 4 of Table 3-1 show that CC% is negative when RHD and RVD increase from IHD and IVD respectively.

3.5 Implementation of Proposed Geometric Correction Schemes

Following sections provide details on implementation and achieved results for proposed geometric correction techniques. The techniques proposed in this thesis are based upon the fact that, prewarping can prevent the geometric distortion [5], [10] and [12]. The effect of prewarping on domain converted captured image $\{I_{DC}\}$ is explained using Figure 3-11. The projected image $\{I_{PD}\}$ without prewarping is shown in Figure 3-11(a). Corresponding captured image is provided in Figure 3-11(b). prewarped projected is shown in Figure 3-11(c) and Figure 3-11(d) shows captured image corresponding to prewarped projected image. What is interesting in these images is that, in Figure 3-11(d) there is no distortion due to projection surface whereas Figure 3-11(b) is highly distorted. This elimination is due to prewarping.

Bezier transformation $\{BT\}$ can also be used to prewarp projected image [12]. Such prewarping

can also counter the geometric distortions induced in the domain converted captured image $\{I_{DC}\}$ by projection surfaces [12]. To apply Bezier transformation on image, Bezier control points should be known as detailed in Appendix A.
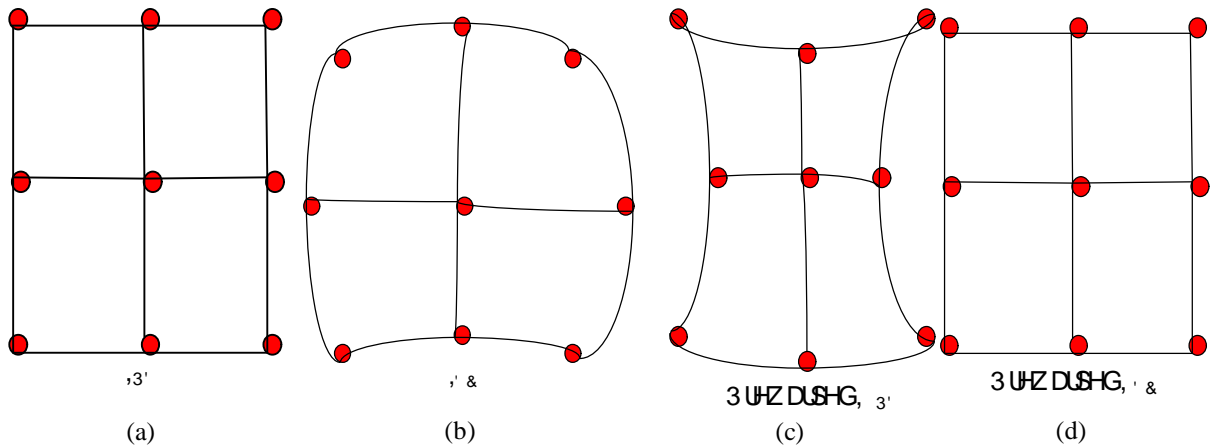
Figure 3-11: Effect of prewarping on domain converted captured image
(a) Projected image $\{I_{PD}\}$ without prewarping, (b) Domain converted captured image $\{I_{DC}\}$ corresponding to without prewarped $\{I_{PD}\}$, (c) Prewarped $\{I_{PD}\}$, (d) $\{I_{DC}\}$ with prewarped $\{I_{PD}\}$.

The problem catered in this work is the calculation of Bezier control points $\{B_{CP}\}$. Summary of implemented approaches is shown in Figure 3-13. The details of implementation algorithm are as followed

1. Two approaches to convert images from camera domain to projector domain were implemented.

    a. Predefined pattern based active approach; in this approach Harris corner detector [33] was used to detect the pattern points in projector domain pattern image $\{P_{PD}\}$ and camera domain pattern image $\{P_{CD}\}$. Based upon these detected corner pattern points homography $\{H\}$ was calculated. Projected pattern points $\{P_{PD}\}$ and captured pattern points $\{P_{CD}\}$ are shown in Figure 3-12(a) and Figure 3-12(b) respectively.

    b. MLSD [29] based passive approach; in this approach SIFT [25] along with MLSD [29] were used to compute homography $\{H\}$. SIFT was used to establish

correspondence between projector and camera domain images. Whereas MLSD was used to estimate corner points from established correspondence between projected and domain converted captured images. Based upon these estimated corner points homography was computed.

2. Two approaches to find Bezier control points $\{B_{CP}\}$ were implemented.

   a. Block matching $\{BBM\}$ based approach; In this approach *MSE, MAE, SSIM, NCC* were used at locations shown in Figure 3-12(c), to calculate projected Bezier feature points $\{B_{PFP}\}$ and captured Bezier feature points $\{B_{CFP}\}$. Then based upon these Bezier feature points $\{B_{FP}\}$ Bezier control points $\{B_{CP}\}$ were calculated and prewarping was done using Bezier transformation $\{BT\}$.

   b. Feature matching based approach; in this approach SIFT [25] was used to establish feature correspondence between projected and domain converted captured images. Based upon this correspondence, MLSD [29] was used to calculate captured Bezier feature points $\{B_{CFP}\}$. Afterwards, Bezier transformation $\{BT\}$ was used to prewarp next projected image.

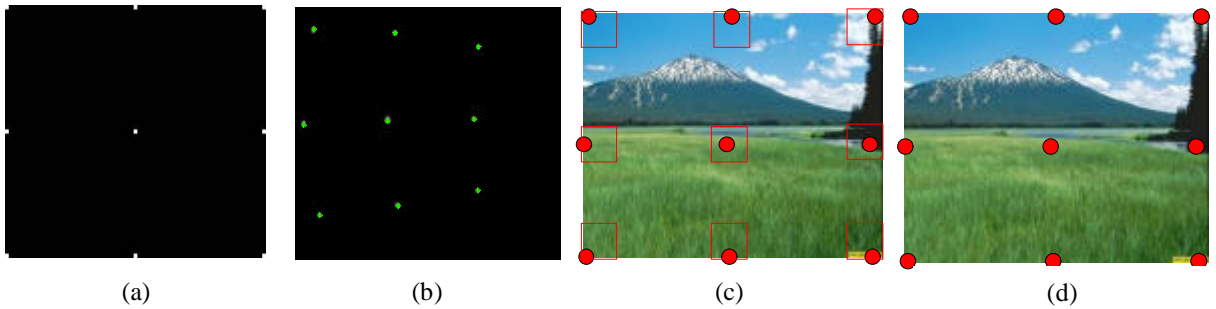(a)   (b)   (c)   (d)

Figure 3-12: Images from different stages of implementation
(a) Projected pattern points $\{P_{PD}\}$, (b) Captured pattern points $\{P_{CD}\}$, (c) Search areas in the image for block based matching, (d) initial position of Bezier control points $\{B_{CP}\}$

Details of the implementation and achieved results are discussed in following sections.

If Passive domain
conversion used

Start

If Active domain
conversion used

Acquire
I_B, I_{CD}, I_{PD}

Acquire
I_B, P_{PD}, P_{CD}

Compute H using
SIFT and MLSD

Compute H using
HARISS corner
detector

Skip prewarping step for
first frame because no B_{CP}
are available beforehand.

Prewarp I_{PD} using
B_{CP}

Acquire
I_{CD}, I_{PD}

Compute I_{DC} using
H

Where

I_B: Background image
ICD: Camera domain image
I_{DT}: Domain converted captured image
IPD: Projector domain image
PPD: Projector domain pattern image
PCD: Camera domain pattern image
H: Homography
MLSD: Moving least squares deformation
SIFT: Scale invariant feature transform
BPFT: Projected Bezier feature points.
BCFP: Captured Bezier feature points.
BBM: Block based matching.
BT: Bezier Transformation
BCP: Bezier control points

If block based
approach used

If feature based
approach used

Establish
correspondence
betwwen I_{PD} and
I_{DC} using SIFT

Compute B_{PFP},
B_{CFP}, using BBM

Compute B_{CFP}
using MLSD

Compute B_{CP}
using B_{CFP} and BT.
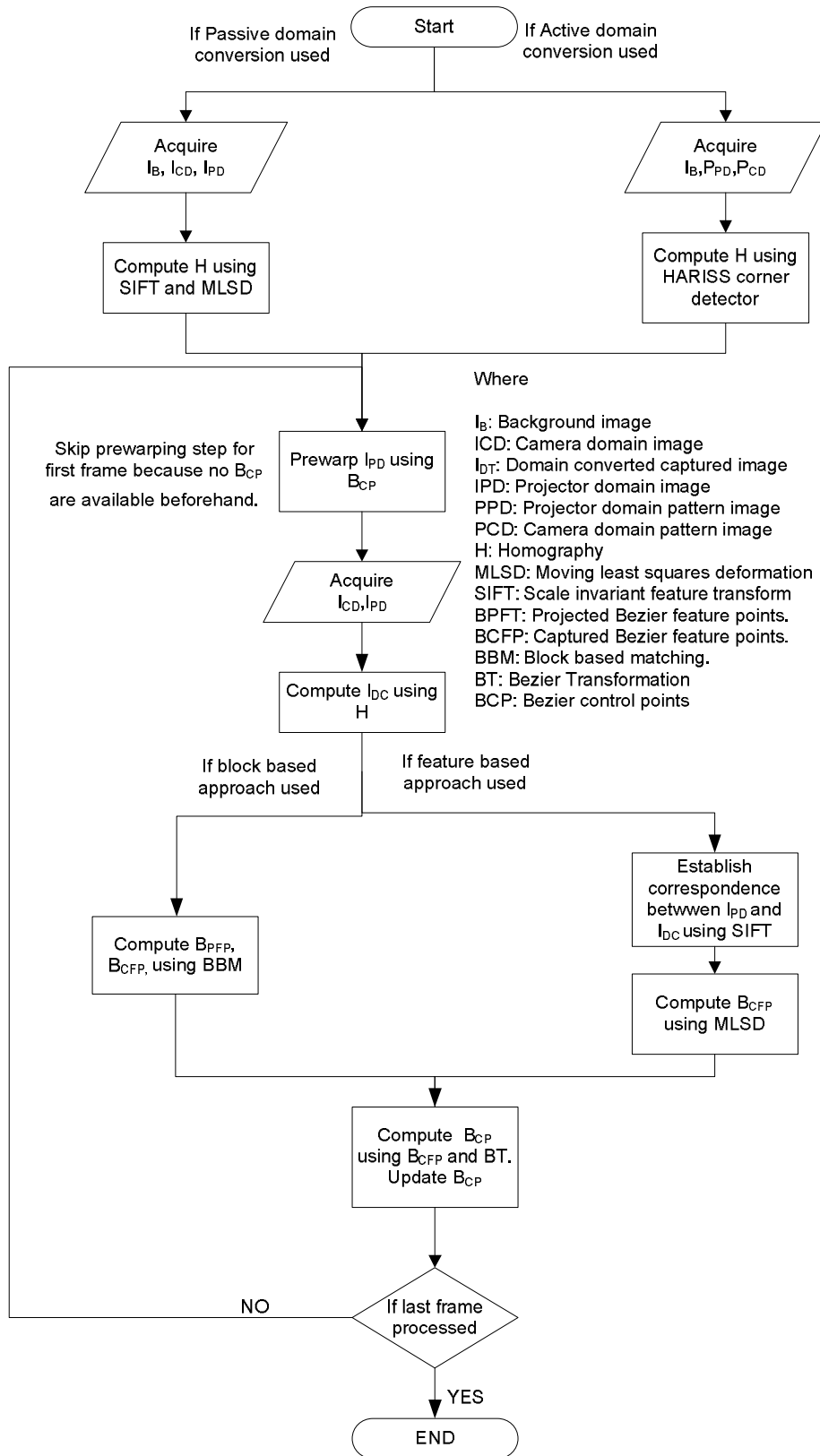Update B_{CP}

NO

If last frame
processed

YES

END

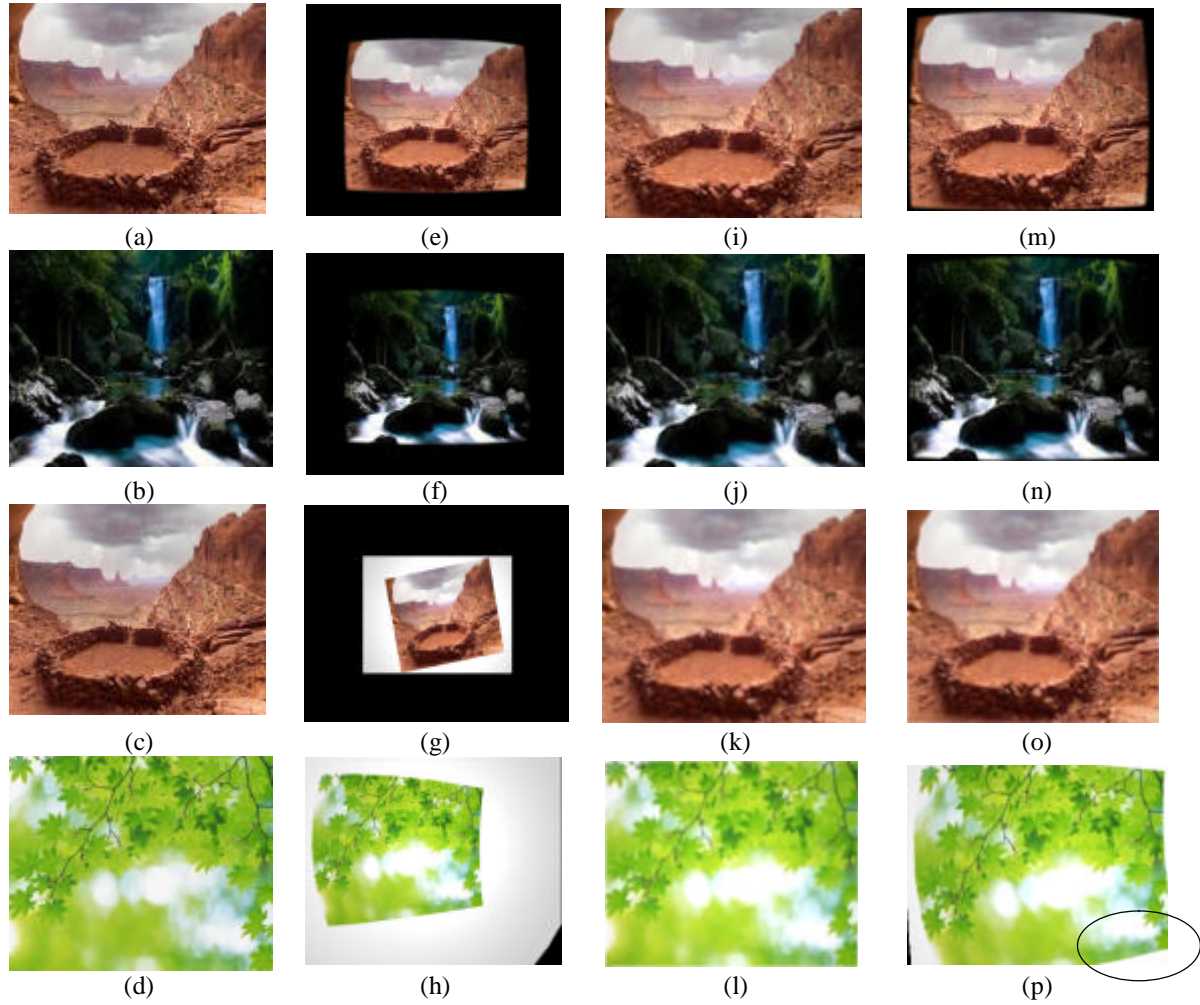**Figure 3-13: Algorithm of implemented geometric correction approaches**

Figure 3-14: Active and passive domain conversion techniques
(a-d) Projector domain image {I_{PD}}, (e-h) Camera domain image {I_{CD}}, (i-l) domain converted captured image {I_{DC}} using active domain conversion, (m-p) domain converted captured image {I_{DC}} using passive domain conversion.

3.5.1 Active and Passive Approaches to Convert Images from Camera to Projector Domain

The camera domain image {I_{CD}} obtained by using both passive and active domain conversion approaches are shown in Figure 3-14. It is visually evident that both Figure 3-14(i-l) and Figure 3-14(m-p) preserve all contents of projector domain image {I_{PD}}, therefore both approaches could be used to compute homography {H}. However advantage of passive approach is that, no predefined pattern is required. Without any predefined pattern for homography {H} calculation, proposed geometric correction technique will become passive online without any offline

projection area estimation phase. One problem with passive domain conversion technique is visible from Figure 3-14(p), right bottom corner of the image (highlighted using circle) is not aligned with the corner of the texture available in Figure 3-14(p). The reason of this misalignment is that, the feature matches from this particular corner gave wrong estimate to MLSD. Use of more robust feature detection and matching algorithm would eliminate this problem.

3.5.2 Approach-I: Block Based Approach for Geometric Correction

In this approach, blocks were identified (see Figure 3-12(c)) in projected images corresponding to locations of Bezier control point. Then exhaustive search method was used to find the match for these blocks in camera domain images. Afterwards, the positions of these blocks were used to determine Bezier control points for Bezier transformation. Matching criterion used for block based techniques were both similarity and difference based [34]. Equation 3-6 to Equation 3-10 gives formulae of used cost functions.

Equation 3-6 represents formula of Sum of Absolute Errors {SAE}. Perfect match using SAE is zero [34].

$$SAE \; ? \; \sum_{i?0}^{N?1} \sum_{j?0}^{N?1} |Curr\_blk_{ij} \; ? \; Ref\_blk_{ij}| \quad \textbf{Equation 3-6}$$

Where

?   Curr_blk is template of captured image

?   Ref_blk is template of projected image

The expression of Mean of Absolute differences {MAE} is given in Equation 3-7. Again perfect match is zero [34].

$$MAE \; ? \; \frac{1}{N^2} \sum_{i?0}^{N?1} \sum_{j?0}^{N?1} |Curr\_blk_{ij} \; ? \; Ref\_blk_{ij}| \quad \textbf{Equation 3-7}$$

The formula of Mean Squared error {*MSE*} is given in Equation 3-8. It is also a difference based measure and it represents perfect match by numeric value of zero [34].

$$MSE \; ? \; \frac{1}{N^2} \sum_{i?0}^{N?1} \sum_{j?0}^{N?1} (Curr\_blk_{ij} \; ? \; Ref\_blk_{ij})^2 \quad \textbf{Equation 3-8}$$

Normalized Cross Correlation {*NCC*} formula is given in Equation 3-9. Values of this measure vary between [-1, 1]. -1 means no match at all on the contrary 1 represents perfect match. In this work, MATLAB Implementation of *NCC* [35] was used.

$$NCC \; ? \; \frac{\sum_{x,y} [f(x,y) \; ? \; \overline{f}(x,y)][t(x \; ? \; u, y \; ? \; v) \; ? \; \overline{t}]}{\{\sum_{x,y} [f(x,y) \; ? \; \overline{f}(u,v)]^2 \sum_{x,y} [t(x \; ? \; u, y \; ? \; v) \; ? \; \overline{t}]^2\}^{0.5}} \quad \textbf{Equation 3-9}$$

? The details of parameters of Equation 3-9 are in [35]

The details of Structural Similarity Index Measure {*SSIM*} [36] formula is given in Equation 3-10. This measure is computationally costly because calculation of complex formulae is required to compute this metric. In this work, MATLAB implementation [37] of SSIM was used.

$$SSIM \; ? \; \frac{(2?_x?_y \; ? \; C1)(2?_{xy} \; ? \; C2)}{(?_x^2 \; ? \; ?_y^2 \; ? \; C1)(?_x^2 \; ? \; ?_y^2 \; ? \; C2)} \quad \textbf{Equation 3-10}$$

? For details of the parameters used in Equation 3-10 refer to [36]

3.5.2.1 Results

In order to assess the applicability of block based matching {*BBM*} approach, it was tested on four test sequences mentioned in section 3.3. Block sizes and search windows were varied and results were checked. Some of the results obtained during experiments are reproduced from Figure 3-15 to Figure 3-19. These graphs are obtained using line based distortion estimation metric of section 3.4. Contrary to expectations, block matching based approach showed inconsistent behavior i.e. algorithm provided geometric correction at some frames whereas it introduced distortion at other frames. The discussion on results is given below.
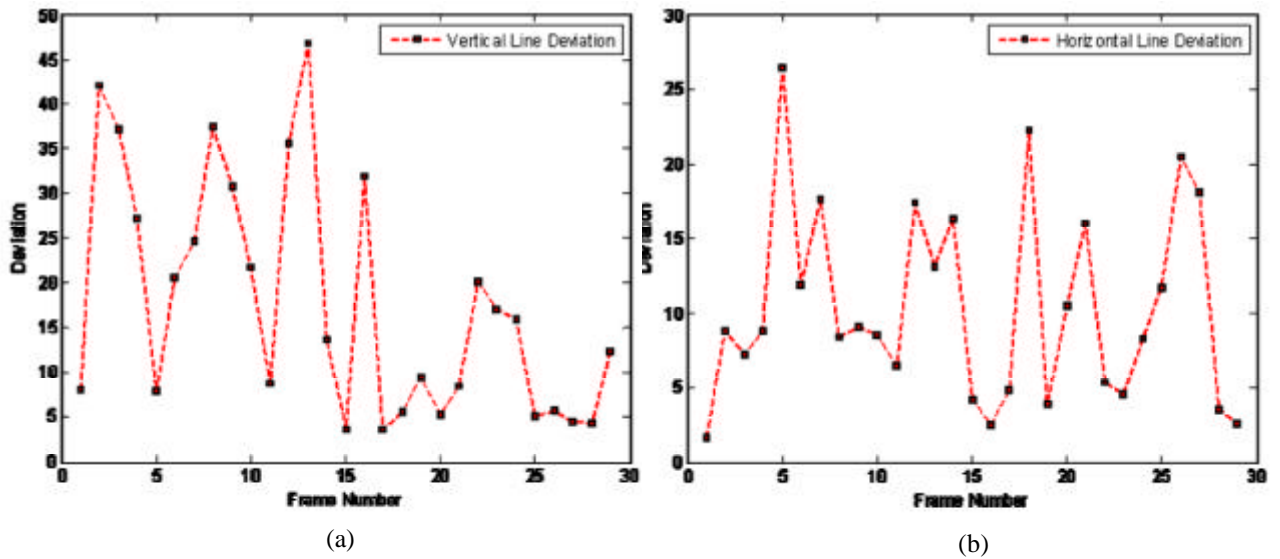
Figure 3-15: Distortion profile of Normalized Cross Correlation based approach
(a) Vertical geometric distortion, (b) Horizontal geometric distortion

Results for block based method using NCC are presented in Figure 3-15. From the data in Figure 3-15(b), it is apparent that for first frame horizontal geometric distortion is 2 whereas it increases to 9 in 2nd frame. At 3rd frame, horizontal distortion reduces to 8 but at 5th frame it increases to 26. From the analysis of trend it can be said that, behavior of algorithm is inconsistent. Same inconsistency is observable in vertical geometric distortion profile of Figure 3-15(a).

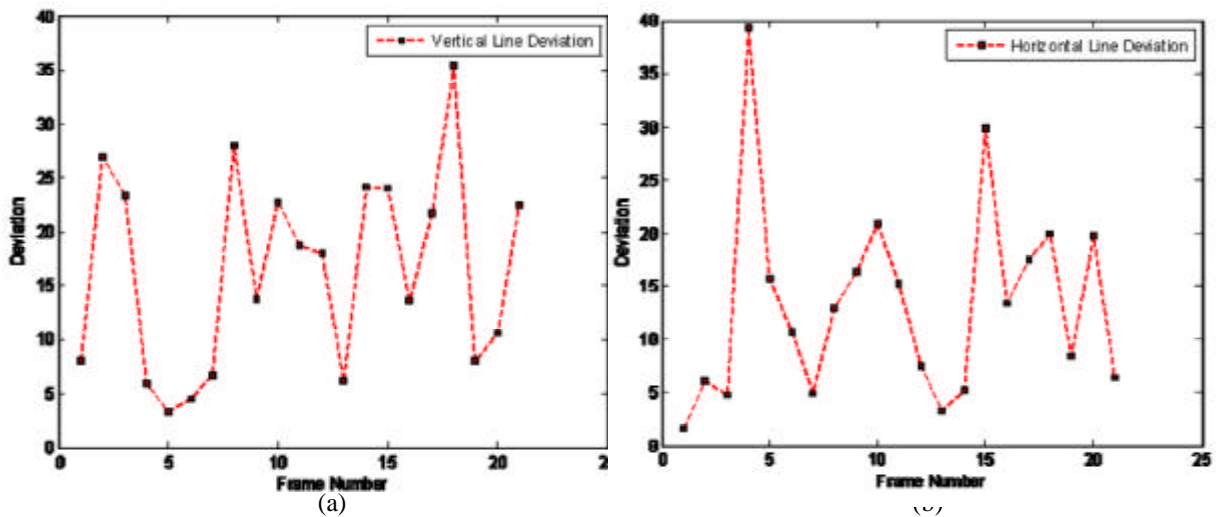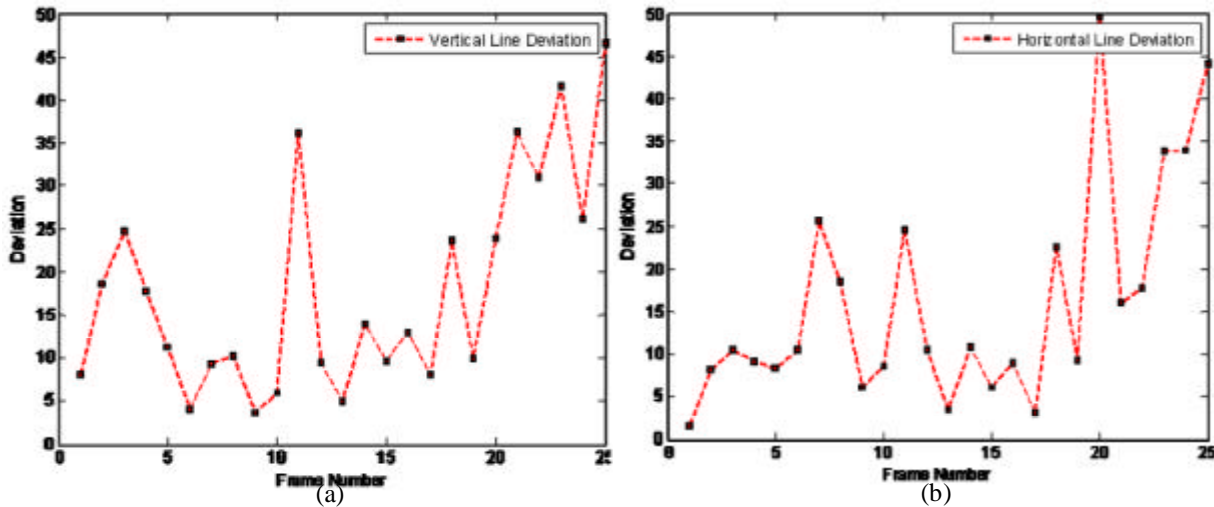**Figure 3-16: Distortion profile of Sum of Absolute Difference based approach**
(a) Vertical geometric distortion, (b) Horizontal geometric distortion

Vertical distortion profile of the algorithm for SAD cost function is shown in Figure 3-16(a).

Initial vertical geometric distortion present in the captured image is 7, after processing of 1st frame algorithm introduces more geometric distortion instead of correction and the vertical geometric distortion goes to 26. At 3rd frame slight correction is achieved. Minimum vertical geometric distortion is achieved at 5th frame but it increases subsequently. Therefore it can be said that, the algorithm is showing inconsistent behavior. Turning now to horizontal geometric distortion profile of Figure 3-16(b), horizontal geometric distortion is 2 at 1st frame. It increases to 6 at second frame whereas slight reduction in geometric distortion is apparent from Figure 3-16(b) at 3rd frame. At 4th frame distortion increases to 40, from these observations it can be concluded that behavior of block matching based algorithm is inconsistent i.e. it is providing geometric correction at some frames but mostly it is inducing more geometric distortions in the processed images.

Figure 3-17: Distortion profile of Mean of Absolute Error based approach
(a) Vertical geometric distortion, (b) Horizontal geometric distortion

The results for MAE cost function are shown in Figure 3-17. Analysis of data present in Figure 3-17(b) yields that, horizontal geometric distortion at 1st frame is 1. It increases to 7 in 2nd frame. Slight geometric correction is achieved in next frames but horizontal geometric distortion increases to 26 at 7th frame. Again the results obtained are inconsistent.
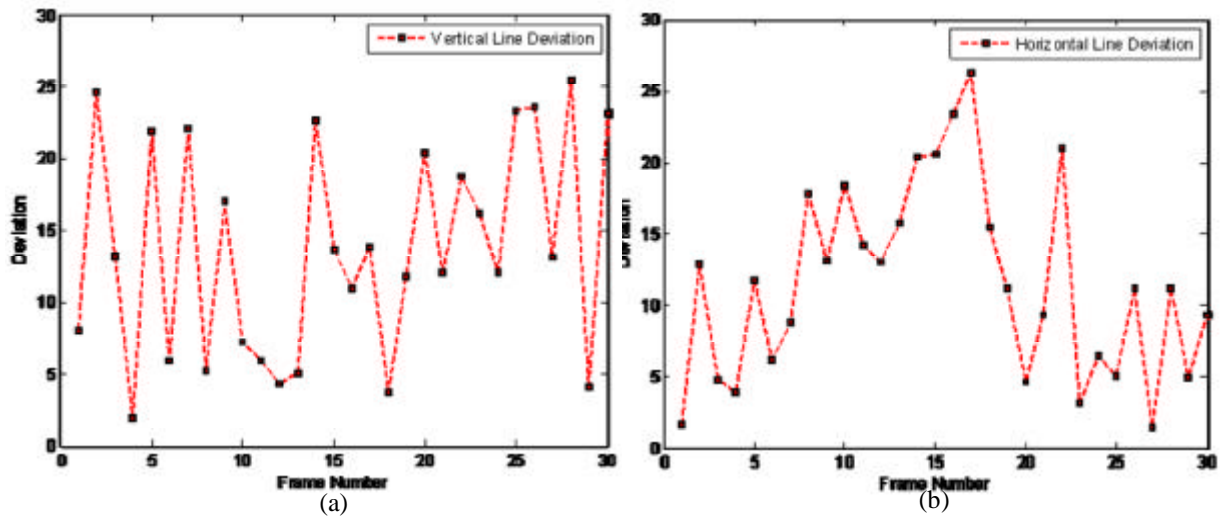
Figure 3-18: Distortion profile of Mean of Squared Error based approach
(a) Vertical geometric distortion, (b) Horizontal geometric distortion

The data present in Figure 3-18 and Figure 3-19 also support the conclusion of "inconsistent behavior" drawn from previous discussion.
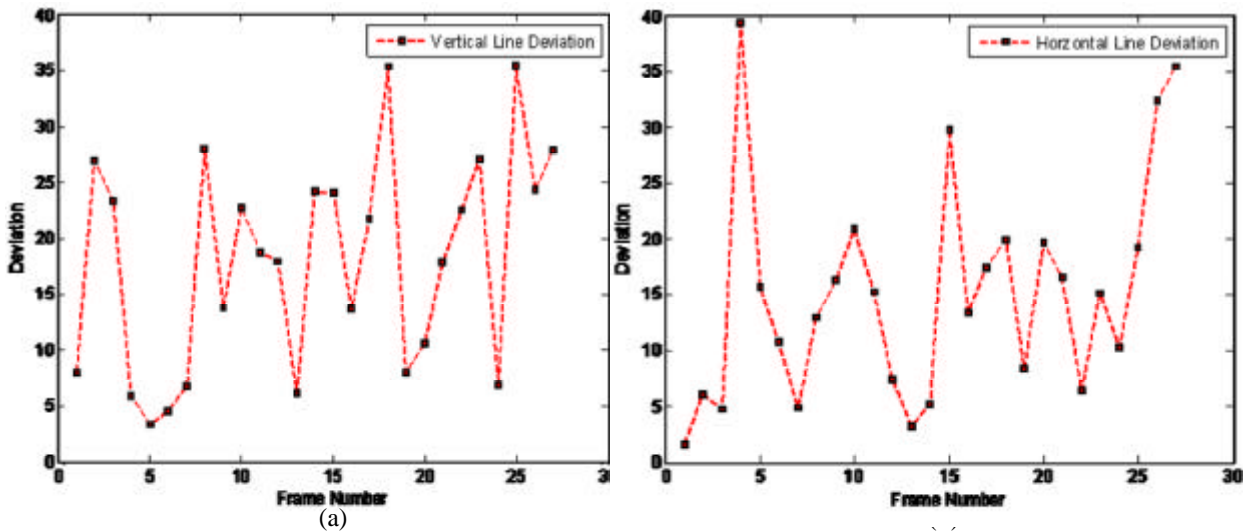
Figure 3-19: Distortion profile of Structural Similarity Index Measure based approach
(a) Vertical geometric distortion, (b) Horizontal geometric distortion

From the discussion on results it can be concluded that, for static quadric surfaces block matching based geometric correction approach fails. It seems possible that, reason of failure is nonlinear rotations and scaling present in the captured images. Since the results obtained for block based matching algorithm are inconsistent, therefore CC% aspect of the results is not

34

analyzed for this technique.

3.5.3 Approach-II: Feature Based Approach for Geometric Correction

To assess feature based approach, both simulation and physical testing environments were employed. For each environment both passive and active techniques were used to compute homography. The breakup of results obtained is as follows

1. Hybrid: Simulation environment

2. Passive: Simulation environment

3. Hybrid: Practical testing environment

4. Passive: Practical testing environment

3.5.3.1 Hybrid: Results of Simulation Environment

Feature based approach using MLSD [11] was tested on all four sequences. The results of algorithm are provided from Figure 3-20 to Figure 3-23 . Interestingly the results obtained are converging and consistent i.e. the distortion reduces after processing of first frame and it remains to minimum levels in subsequent frames. The discussion on results is given below.

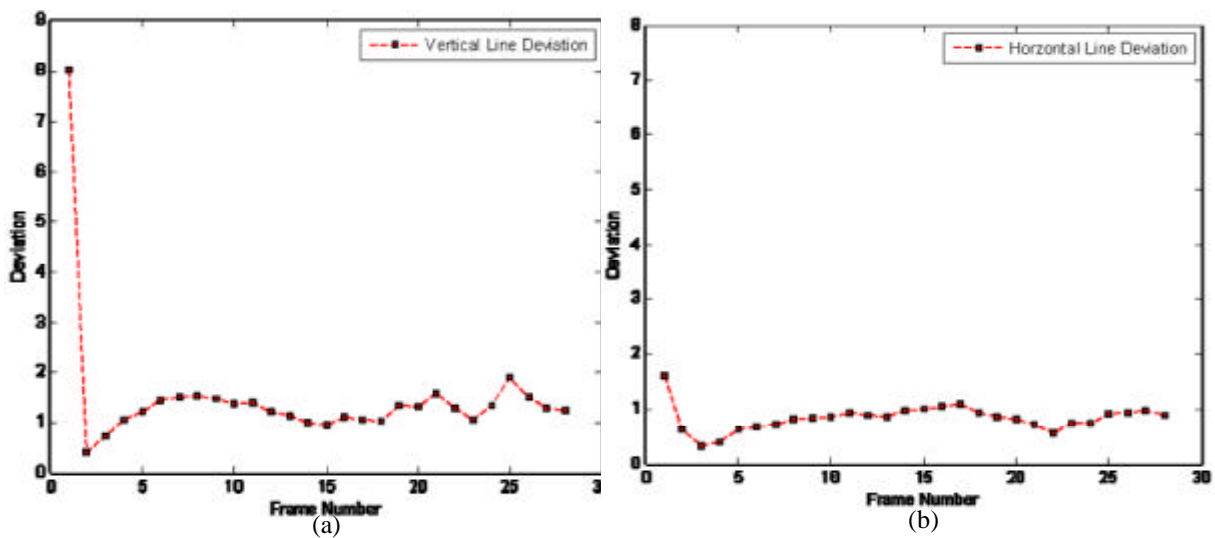**Figure 3-20: Distortion profile of hybrid geometric correction, walk sequence**
(a) Vertical geometric distortion, (b) Horizontal geometric distortion

35

As detailed in section 3.4, calculated horizontal and vertical geometric distortions can be used to analyze the behavior of geometric correction algorithm. Such geometric distortion profile of proposed hybrid geometric calibration algorithm for walk sequence is provided in Figure 3-20. It is apparent from Figure 3-20(a) that, vertical geometric distortion present in 1st frame is 8 whereas it reduces to 0.5 in second frame. Maximum vertical geometric distortion after first geometric correction is 2, which occur at 25th frame. Comparison of geometric distortions of 25th frame and 1st frame reveals that ($\frac{?}{?}*100 = 25\%$) 25% of distortion is present in captured image, which implies that algorithm has eliminated minimum 75% vertical geometric distortion from the image. Turning now to Figure 3-20(b), it is apparent that initial distortion is 1.8 and maximum subsequent distortion is 0.9 at 17th frame, so overall horizontal geometric correction achieved is 50%. From the data available in Figure 3-20, CC% introduced in Equation 3-5 of section 3.4 can also be calculated. The CC% calculation is given below

$$CC\% \ ? \ (1 \ ? \ \frac{\frac{0.9}{1.8} \ ? \ \frac{2}{8}}{2})*100 \ ? \ 62.5\%$$
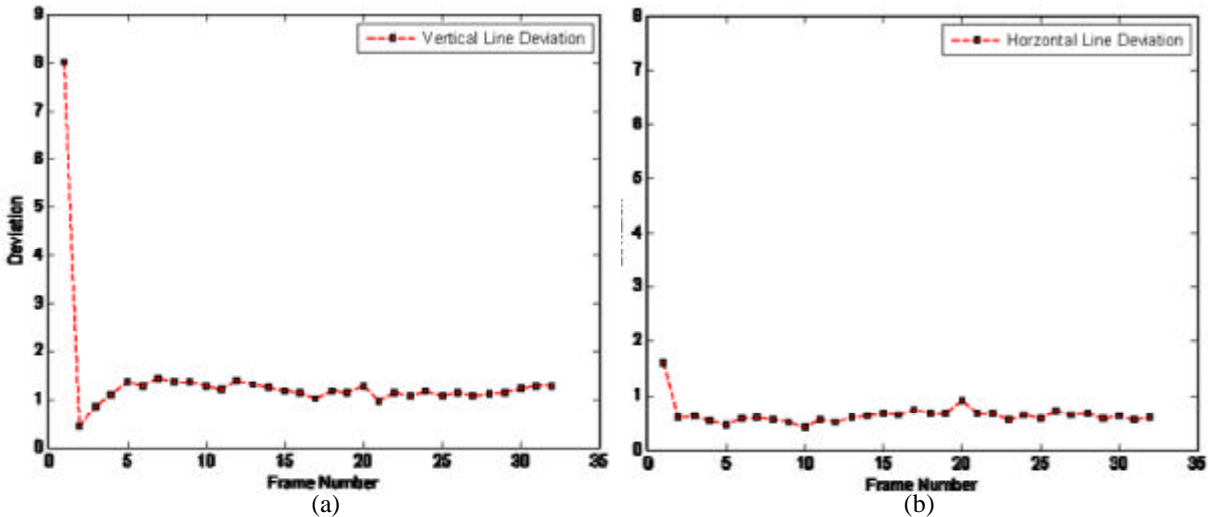

Figure 3-21: Distortion profile of hybrid geometric correction, waterfall sequence
(a) Vertical geometric distortion, (b) Horizontal geometric distortion

Results for waterfall sequence are presented in Figure 3-21. Analyzing Figure 3-21(a) yields that, initial vertical geometric distortion present in 1st frame is 8, it reduces to 0.5 in second frame and afterwards there is slight increase in vertical distortion. Maximum vertical geometric distortion in subsequent frames is 1.25, which occurs at frame number 7. This is 15% of initial distortion so it can be said that, algorithm has reduced 85% vertical geometric distortion from the image. Whereas Figure 3-21(b) reveals that, algorithm removed 50% horizontal geometric distortion because initial horizontal geometric distortion is 1.8 and maximum geometric distortion afterwards is 0.9 at 20th frame. The data of Figure 3-21 is also used to calculate CC%, which is 67.5%. Detailed analysis of CC% for all test sequences is provided in Figure 3-24.
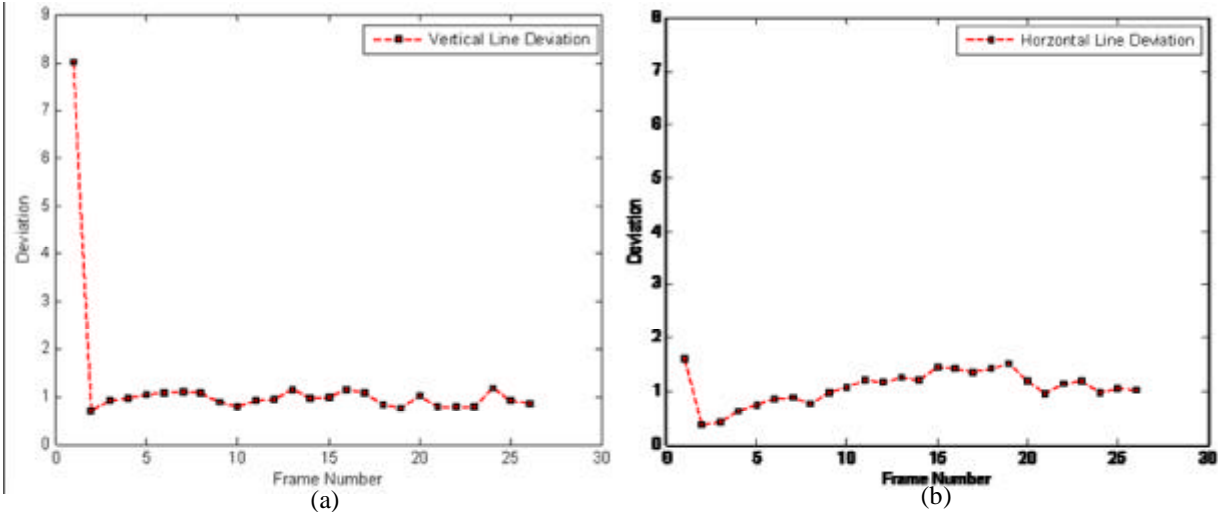

(a)   (b)

Figure 3-22: Distortion profile of hybrid geometric correction, bus sequence
(a) Vertical geometric distortion, (b) Horizontal geometric distortion

Figure 3-22(a) shows vertical geometric distortion profile for bus sequence. Analysis of data present in the graph yields that, vertical distortion in uncorrected image is 8, it reduces to 0.75 in second frame. Maximum distortion occurs at 24th frame which is 1.25. So again it can be said that, algorithm achieved minimum 85% vertical geometric correction for bus sequence. Moving to Figure 3-22(b), initial horizontal geometric distortion is 1.8 and afterwards maximum geometric distortion is 1.7 which yields that only 4% distortion is removed. The value of CC%
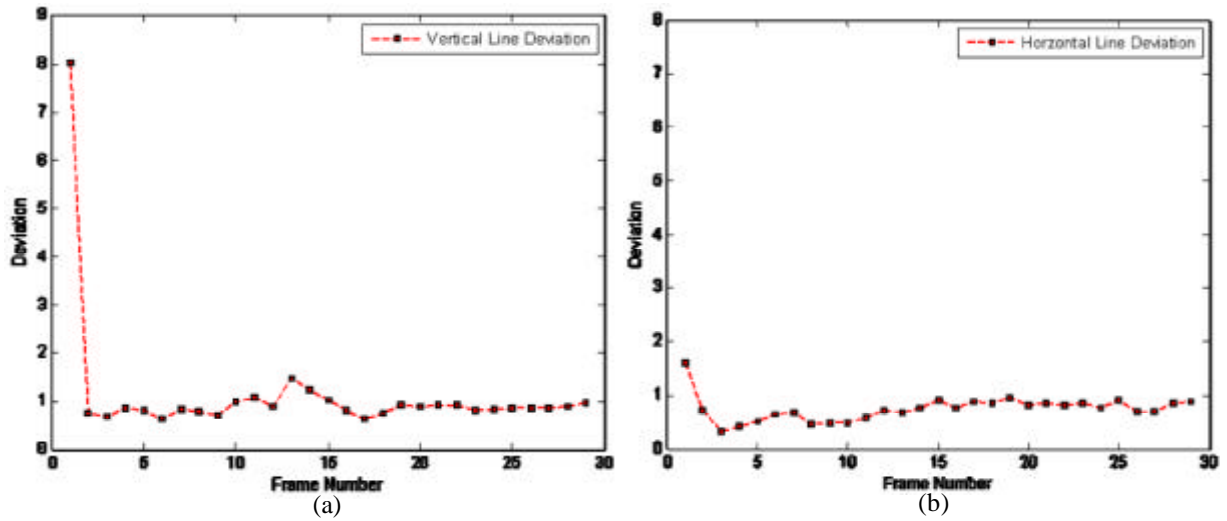
37

calculated using data of Figure 3-22 is 71.35%.

Figure 3-23: Distortion profile of hybrid geometric correction, driving sequence
(a) Vertical geometric distortion, (b) Horizontal geometric distortion

Results for driving sequence are shown in Figure 3-23. Considering Figure 3-23(b), horizontal geometric distortion in 1st uncorrected image is 1.75. It reduces to 0.75 in 2nd frame and remains to such level afterwards. It can be established that, algorithm achieves minimum horizontal geometric correction of 58% for driving sequence. Vertical correction achieved is 82% because initial vertical geometric distortion was 8 and maximum vertical distortion afterwards was 1.5 at 13th frame, as shown in Figure 3-23(a). The calculated value of CC% is 69.79%.

3.5.3.1.1 Cumulative Percentage of Correction for Hybrid Approach

The CC% summary of results for simulation environment is reproduced in Figure 3-24. It is apparent from the figure that CC% value for all video sequences is between 50% and 85%. The minimum CC% value is obtained for bus sequence at 19th frame. Such low value of correction is probably due to, lack of feature points in frames (for which low values of CC% are achieved) of the sequence or feature mismatch at some points. However this low value of CC% is the worst case being considered, cumulative correction values for other sequences in the CC% profile are greater than 60%.
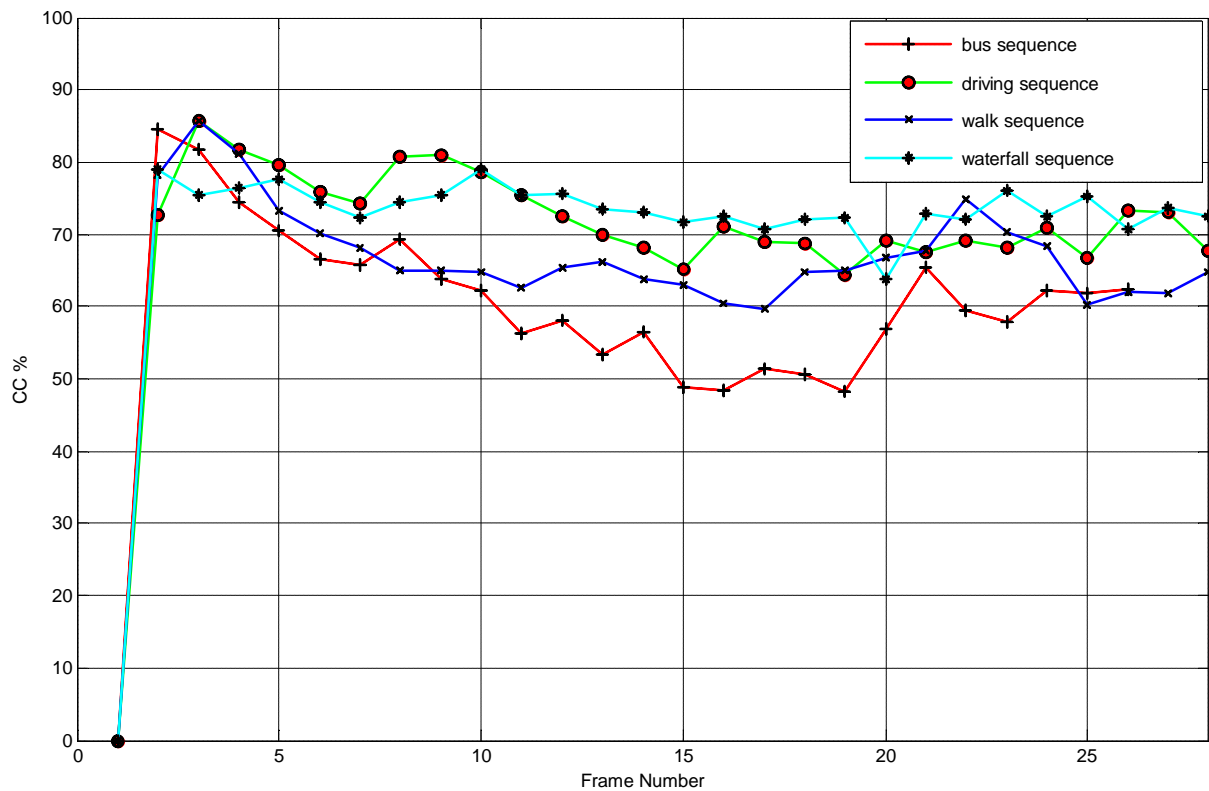
Figure 3-24: CC% summary of hybrid approach

| (a) | (b) | (c) | (d) |

| (e) | (f) | (g) | (h) |
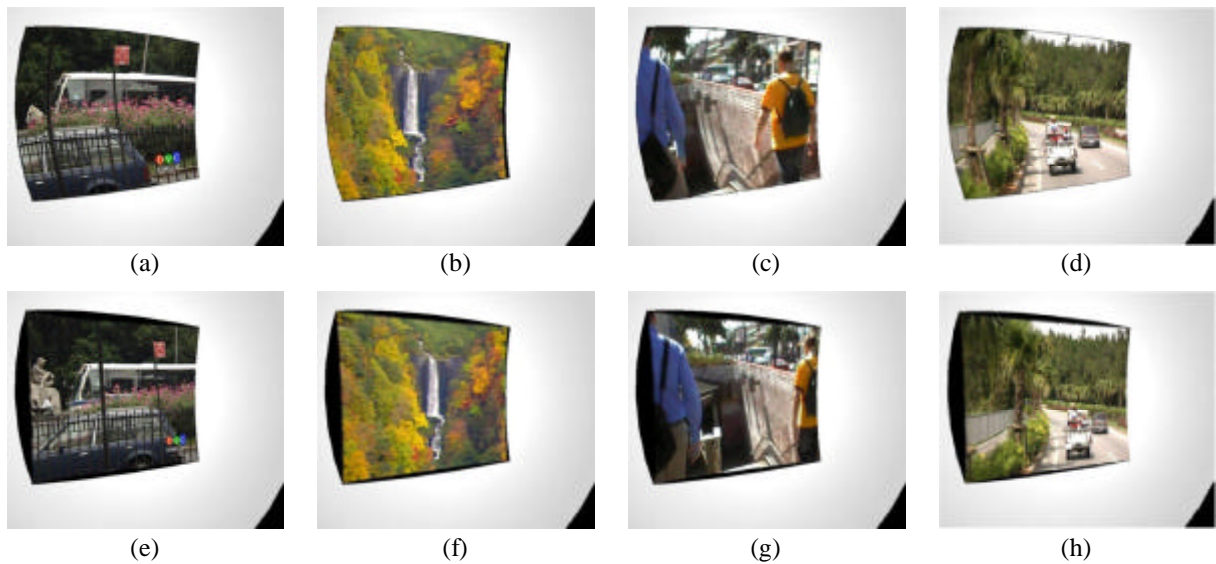
Figure 3-25: Image profile for hybrid geometric correction
(a-d) Initial uncorrected images, (e-f) Final corrected image

To do visual inspection of geometric correction achieved, the images from video sequences are also reproduced in Figure 3-25. In Figure 3-25(a-d) original uncorrected images are presented

whereas in Figure 3-25(e-f), final geometrically corrected images are shown. It is visually evident that, Figure 3-25(a-d) has geometric distortion and this distortion is considerably suppressed in Figure 3-25(e-f).

3.5.3.2 Passive: Results of Simulation Environment

Passive online approach was also tested on four sequences in simulation environment. The obtained results are given from Figure 3-26 to Figure 3-29. The results are comparable to those of hybrid approach in terms of convergence and consistency. Analysis of obtained results is given below.

(a)   (b)

Figure 3-26: Distortion profile of passive geometric correction, walk sequence
(a) Vertical geometric distortion, (b) Horizontal geometric distortion

Figure 3-26(a) shows that, vertical geometric distortion present in first frame is 8 whereas it is 1.5 in 2nd frame and in all subsequent frames it remains at such minimum level. Maximum vertical geometric distortion recorded after 1st correction is 2 which occur at 43rd frame. Comparison of 43rd frame and 1st frame reveals that 25% of vertical distortion is present in captured image, which implies that algorithm has eliminated minimum 75% vertical distortion from the image. If Figure 3-26(b) is analyzed, it is apparent that initial distortion is 1.2 and maximum subsequent distortion is 1.1 at 35th frame, so overall horizontal geometric correction achieved is 8%. Calculated value of CC% for this set of results is 57%.
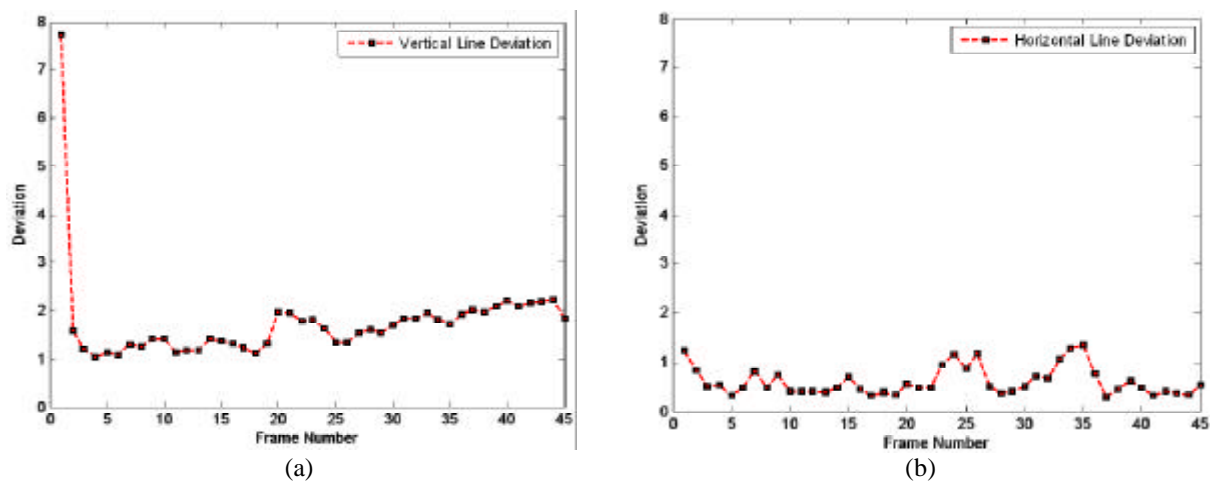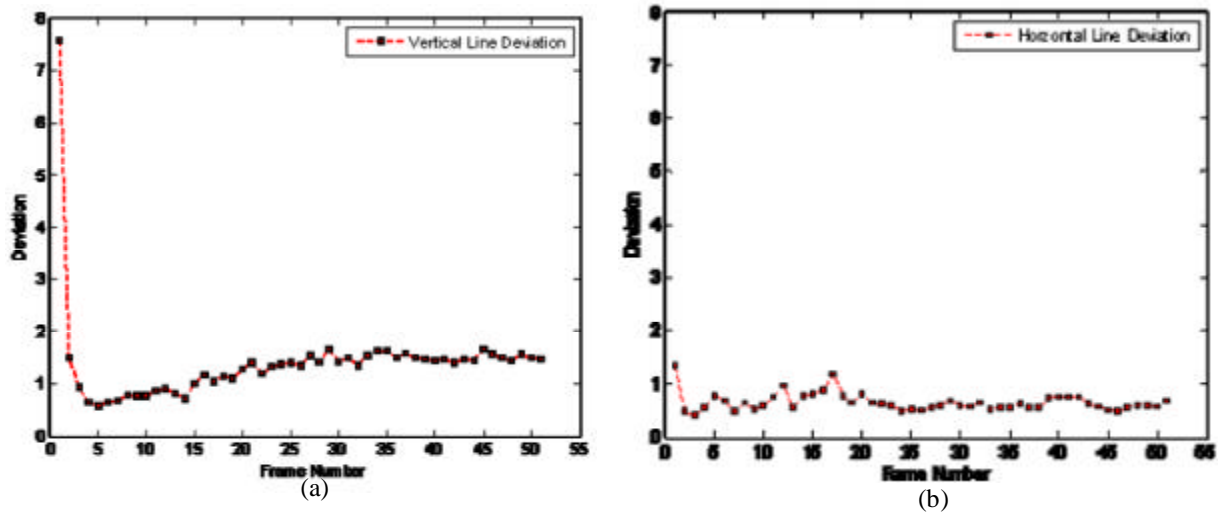
Figure 3-27: Distortion profile of passive geometric correction, waterfall sequence
(a) Vertical geometric distortion, (b) Horizontal geometric distortion

Results for waterfall sequence are presented in Figure 3-27. Analysis of Figure 3-27(a) yields that, initial vertical geometric distortion present in 1st frame is 8, it reduces to 1.5 in 2nd frame and afterwards there is slight increase in distortion. Maximum distortion in subsequent frames is 1.6 which occurs at frame number 29. This is 20% of initial geometric distortion so it can be said that, algorithm has reduced 80% vertical distortion from the image. Considering Figure 3-27(b), initial horizontal geometric distortion is 1.25 whereas maximum subsequent geometric distortion is 0.9 at 18th frame. Therefore overall horizontal geometric correction achieved is 28%. CC% for the data available in Figure 3-27 is given below

$$CC\% \ ? \ (1\ ? \ \frac{\frac{0.9}{1.25}\ ? \ \frac{1.6}{8}}{2})*100 \ ? \ 54\%$$

41

Figure 3-28: Distortion profile of passive geometric correction, bus sequence
(a) Vertical geometric distortion, (b) Horizontal geometric distortion

Vertical geometric distortion profile for bus sequence is shown in Figure 3-28(a). Analysis of data yields that, vertical geometric distortion present in uncorrected image is 8. Maximum vertical distortion occurs at 31st frame which is 3. So again it can be said that, algorithm achieves minimum 64% vertical geometric correction. It is indicated in Figure 3-28(b) that, initial horizontal geometric distortion is 1.25 whereas maximum subsequent distortion is 1.1 at 15th frame. Overall horizontal geometric correction achieved is 18% and calculated CC% is 37%.
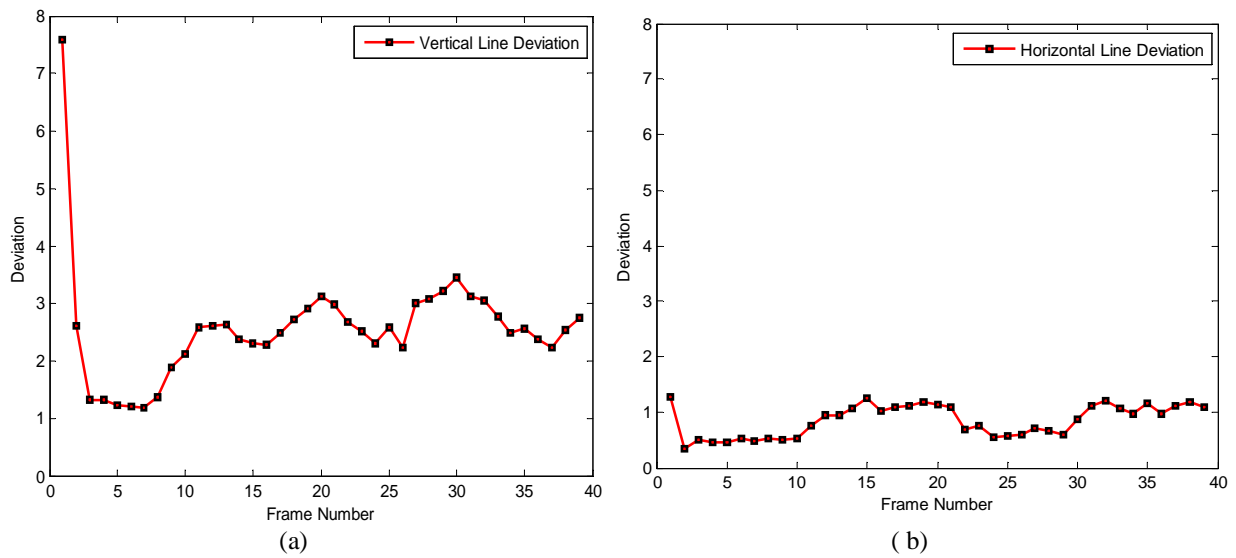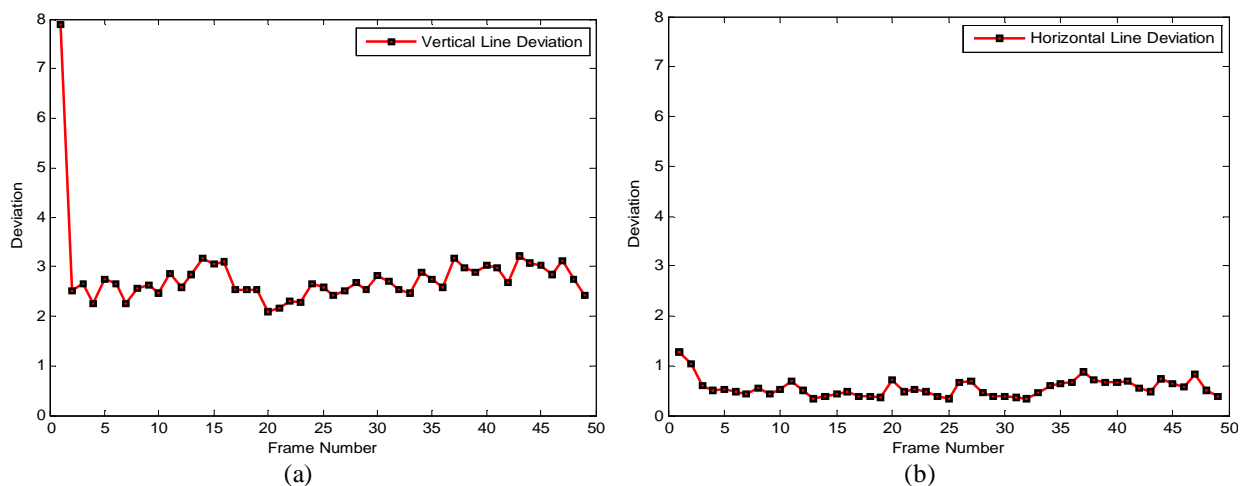

Figure 3-29: Distortion profile of passive geometric correction, driving sequence
(a) Vertical geometric distortion, (b) Horizontal geometric distortion

Distortion profile for driving sequence is shown in Figure 3-29. Analysis of data present in Figure 3-29(b) yields that, horizontal geometric distortion in 1st uncorrected image is 1.25. Geometric distortion reduces to 1.0 in 2nd frame and remains to such level afterwards. It can be seen from Figure 3-29 that, algorithm achieves minimum horizontal geometric correction of 60% for driving sequence because maximum distortion after 1st frame occurs at 3rd frame i.e. 0.5. Vertical geometric correction achieved is 64% because initial vertical geometric distortion is 8 and maximum vertical distortion afterwards is 3, which occurs at 14th frame, as shown in Figure 3-29(a).

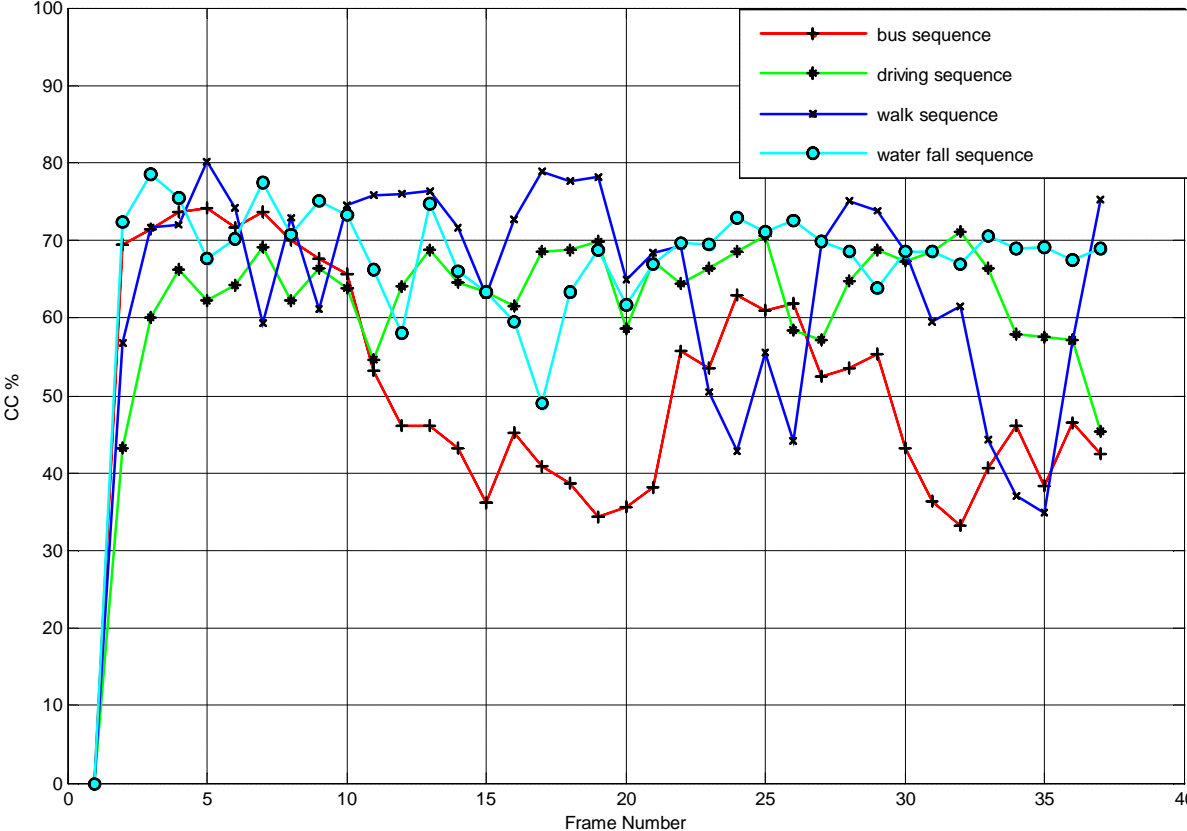**3.5.3.2.1 Cumulative Percentage of Correction for Passive Approach**

Figure 3-30: CC% summary of passive approach

Summary of CC% values for simulation environment is provided in Figure 3-30. It is apparent from data present in the Figure 3-30 that, CC% value for all video sequences is between 40% and

80%. Minimum value of CC% is recoded for bus sequence at 32nd frame. Such low value of correction is probably due to lack of feature points in frames (for which low values of cumulative correction are achieved) of the sequence or feature mismatch at some points. However one fact is still encouraging that, algorithm did not introduce any severe distortion in any image. Moreover this low value of CC% is the worst case being considered, distortion values for other sequences in the distortion profile are greater than 50%. One observation from Figure 3-30 is that, CC% values undergo fluctuations for some frames (15th and 30th frame of bus sequence). The probable reason of these fluctuations can be small number of matching features at these frames. Another reason can be that, proposed algorithm calculates Bezier parameters using feature matches of current frame instead of using average of Bezier parameters of current and previous frames.

| (a) | (b) | (c) | (d) |

| (e) | (f) | (g) | (h) |
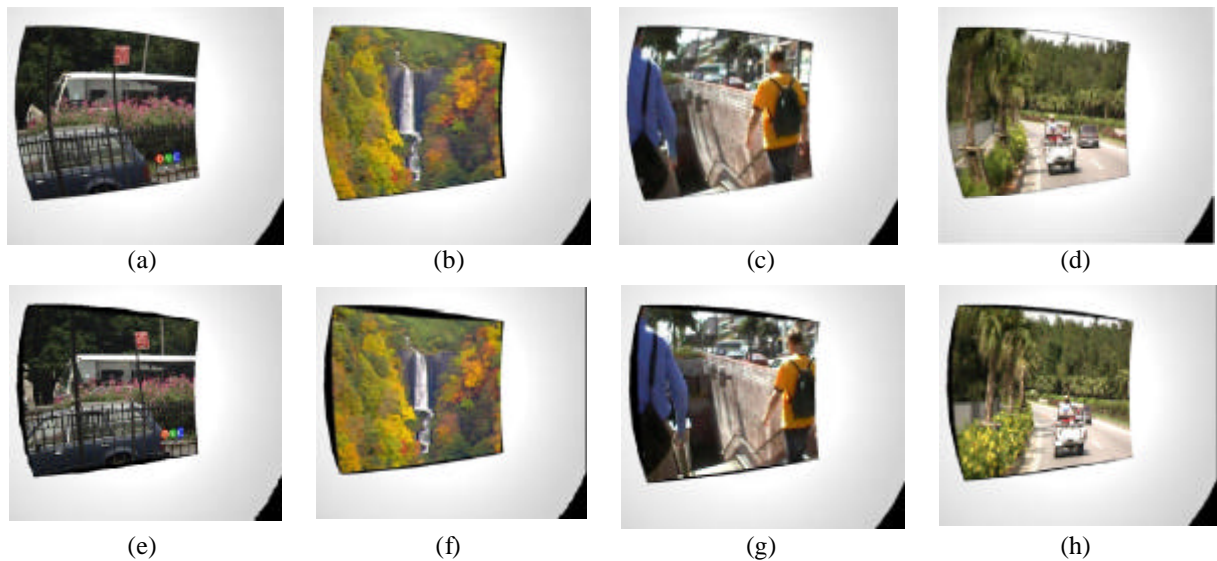
Figure 3-31: Image profile for passive geometric correction
(a) Initial uncorrected images, (b) Final corrected image

To do visual inspection of geometric correction achieved, the images from test sequences are reproduced in Figure 3-31. In Figure 3-31(a-d) uncorrected images are presented whereas in Figure 3-31(e-h) final geometrically corrected images are shown. It is visually evident that, Figure 3-31(a-d) has maximum distortion and this distortion is suppressed in Figure 3-31(e-h).

3.5.3.3 Hybrid: Results of Physical Environment

To validate, algorithm was checked on practical testing setup. Setup used consists of projector NEC M420x and a digital camera Cannon 420-D. For conversion matrix (Homography) calculation, pattern based approach was used. The results obtained are presented in Figure 3-32. Uncorrected images are shown in Figure 3-32(a-d) whereas geometrically corrected images are illustrated in Figure 3-32(e-h).

| (a) | (b) | (c) | (d) |

| (e) | (f) | (g) | (h) |
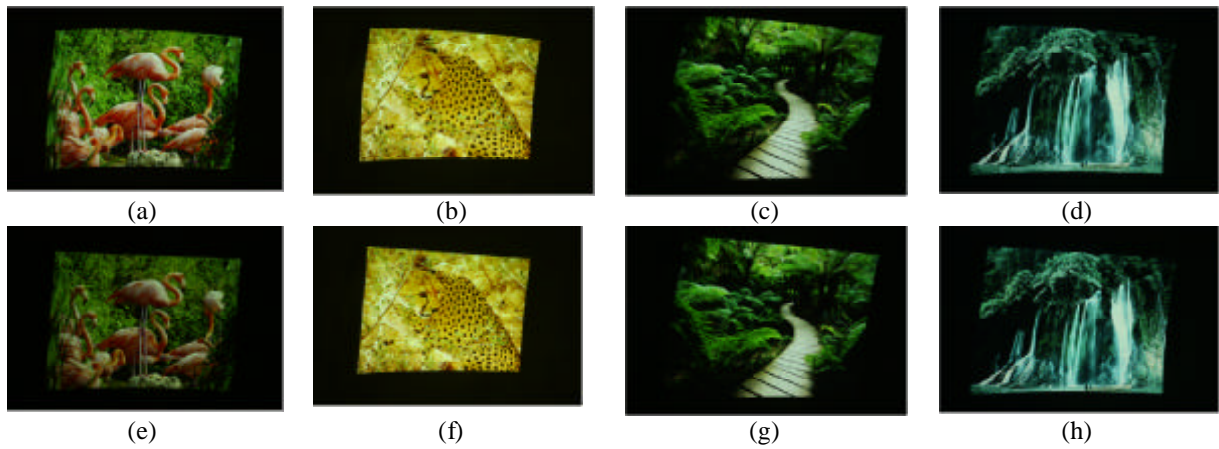
Figure 3-32: Image profile for hybrid geometric correction, tested in real setup
(a-d) Uncorrected Image, (e-h) Geometrically corrected image

The amount of correction achieved is not very evident visually. However if the achieved corrections are quantified using distortion estimation metric of section 3.4, the amount of correction achieved can be investigated. The quantified results are shown in Table 3-2.

Table 3-2: Quantified results using hybrid geometric correction technique

Image No.	Initial horizontal distortion	Reduced horizontal distortion	Initial vertical distortion	Reduced vertical distortion	CC%
image 1	25.9974	13.4355	106.9027	57.9512	47.05527
image 2	27.0581	15.0593	100.7497	63.6955	40.56152
image 3	28.4083	7.5588	48.1689	28.1769	57.44812
image 4	30.8889	16.1751	115.8549	45.2901	54.27125

Minimum CC% achieved is 40% as apparent from Table 3-2. This is acceptable because algorithm showed consistent behavior in simulation phase. Moreover the CC% achieved depends mainly on the number of features extracted from the images i.e. small number of feature matches

in the area of interest (area of image corresponding to Bezier control points) will yield low CC%.

3.5.3.4 Passive: Results of Physical Environment

To check the applicability of passive geometric correction approach in real environment, setup similar to section 3.5.3.2 was used. The results obtained are presented in Figure 3-33
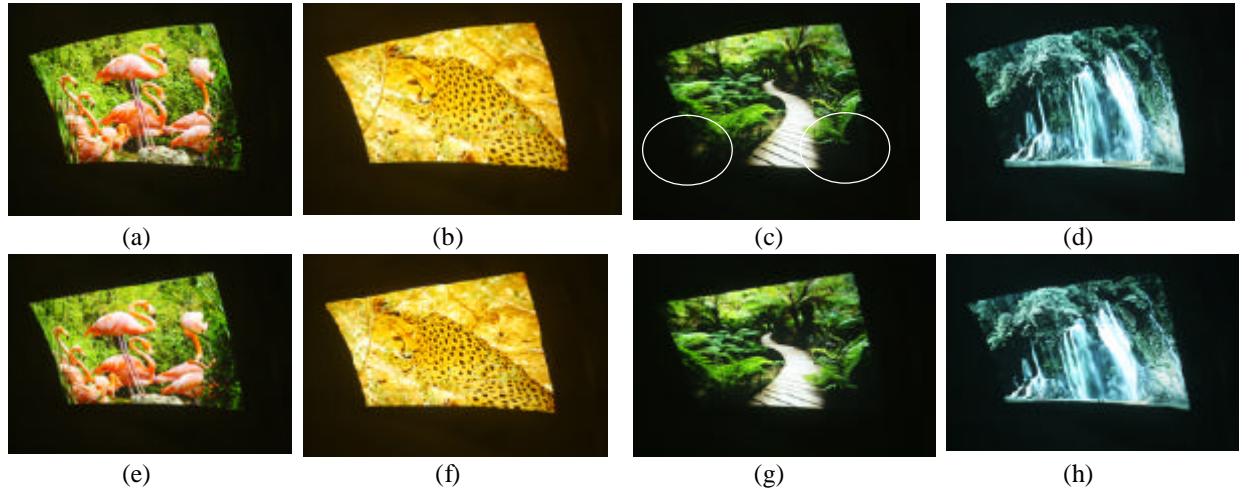

Figure 3-33: Image profile for passive geometric correction, tested in real setup
(a-d) Uncorrected Image, (e-h) Geometrically corrected image

Again visual analysis was hard to do, so same CC% metric was used to determine the geometric correction. The quantified results are reproduced in Table 3-3. It is apparent from the table that, minimum correction achieved using passive online geometric correction approach is 32%. This reduction in CC% suggests that, proposed hybrid technique is better than passive online geometric correction technique. However the advantage of latter is that, it does not required offline display area estimation.

Table 3-3: Quantified results using passive geometric correction technique

Image No.	Initial horizontal distortion	Reduced horizontal distortion	Initial vertical distortion	Reduced vertical distortion	CC%
image 1	91.6481	51.1077	860.3147	456.2763	45.599437
image 2	91.6481	49.9019	860.3147	630.8514	36.111277
image 3	91.6481	59.7054	860.3147	605.8139	32.217966
image 4	91.6481	47.5942	860.3147	521.5049	43.725468

One important observation from Table 3-2 and Table 3-3 is that, CC% value of hybrid approach

is 57% whilst it is 32% for passive approach. This difference in CC% is due to absence of matching features in encircled parts of the Table 3-3(c) i.e. image 3. Likewise, if small number of matching features is present in an image, CC% value of passive approach for that particular image will be small.

3.5.3.5 Comparison: Proposed Hybrid and Passive Approaches

Comparison of proposed approaches for four test sequences is reported in Figure 3-34. To perform the comparison, CC% per frame for each test sequence was calculated. Then average of these CC% values per frame for all test sequences was plotted against frame number. Same procedure was used for both approaches and resulting average CC% is shown in Figure 3-34. It is evident from Figure 3-34 that on average hybrid approach performs better. However, advantage of passive approach is that it requires no offline display area estimation phase.
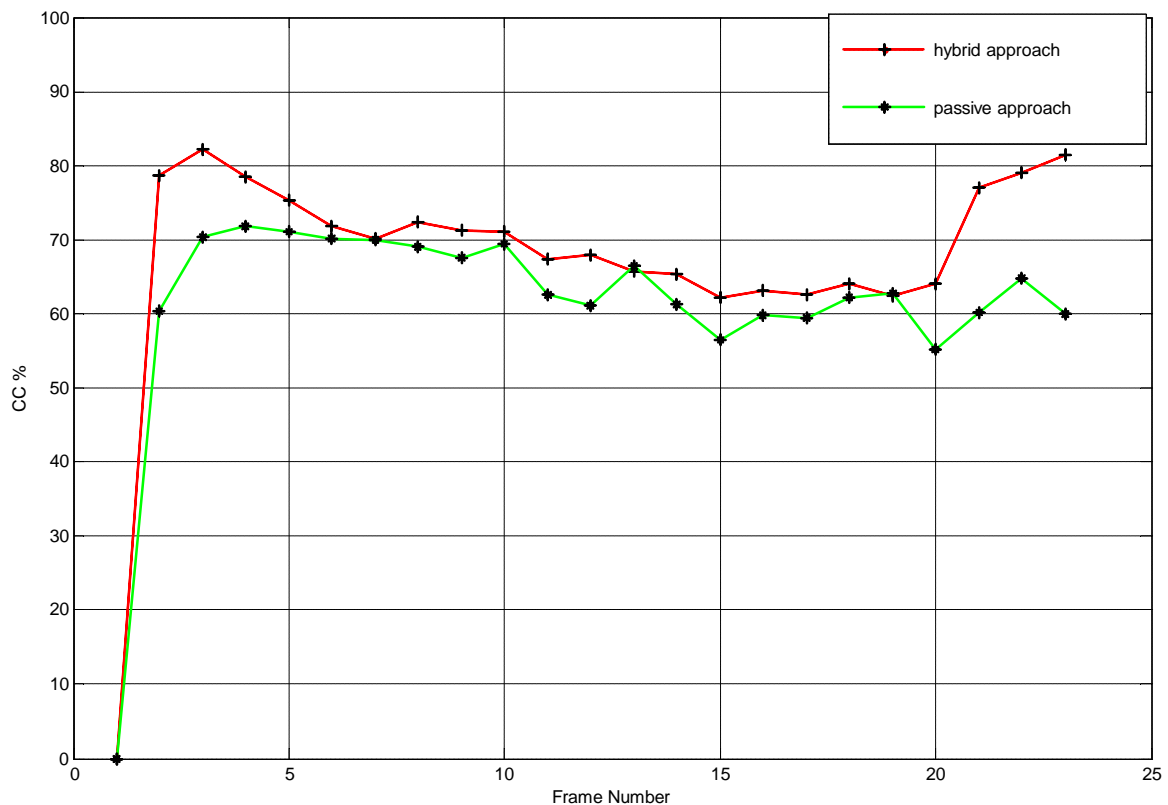

Figure 3-34: comparison of proposed hybrid and passive approaches

3.5.4 Fixed Corner Point Dynamic Surfaces

In order to assess applicability of proposed algorithm on fixed corner point dynamic surfaces (algorithm cannot adapt moving corner point dynamic surface because proposed hybrid approach requires offline homography calculation phase and proposed passive online algorithm calculates homography at first frame only), several surfaces were designed in 3ds Max and using these surfaces, fixed corner point dynamic surface was simulated. Figure 3-35 gives simulation result for driving sequence.

3.5.4.1 Results: Hybrid Geometric Calibration

The results obtained from preliminary analysis of the approach are shown in Figure 3-35. Vertical graph cutting lines in Figure 3-35 are provided to highlight the instance at which surface was changed. As can be seen from Figure 3-35(a), initial vertical geometric distortion is 5 after first iteration distortion reduces to 1.6. It increases slightly in 3rd frame. According to algorithm of Figure 3-6, after 3rd frame surface is changed, so geometric distortion increases to 8 due to surface change. At 5th frame again distortion is reduced to 1.2. In this fashion, after every surface change geometric distortion increases significantly, however at next frame algorithm eliminates the distortion. Considering Figure 3-35(b), initial horizontal geometric distortion is 4, algorithm reduces this distortion to 1.5 after processing of first frame and after second frame horizontal distortion is 1. Projection surface is changed at 4th frame resulting in increased distortion of 4, again algorithm removes the geometric distortion and it reduces to 0.7. In this way the distortions are eliminated from the domain converted captured images after every surface change. From this discussion it can be concluded that proposed algorithm can be used to tackle the problem of geometric correction of fixed corner point dynamic surfaces.
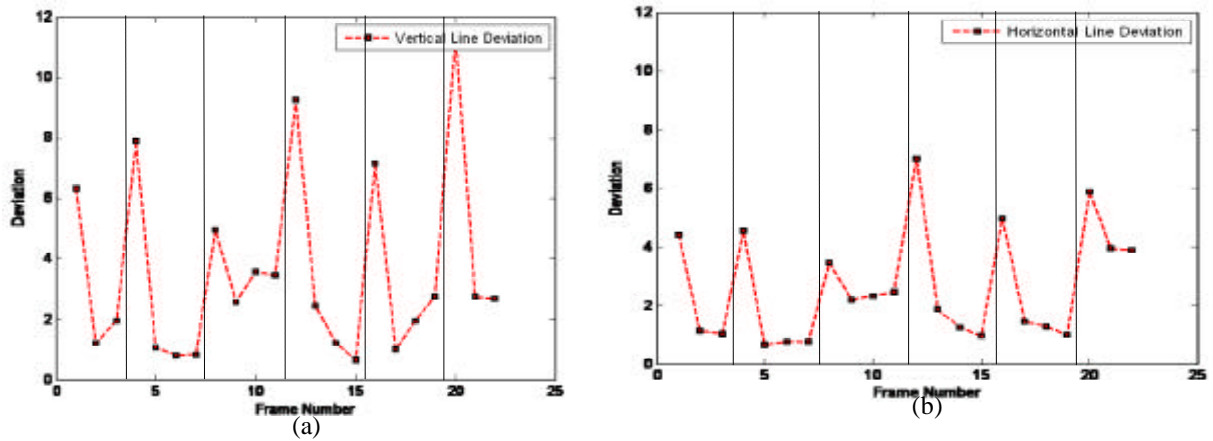
Figure 3-35: Distortion profile for hybrid geometric correction, fixed corner point dynamic surface
(a) Vertical geometric distortion, (b) Horizontal geometric distortion

3.5.4.2 Results: Passive Online Geometric Calibration

To extend the scope of proposed passive online geometric calibration algorithm, it was also tested on fixed corner point dynamic surfaces. The results obtained in simulation environment are surprisingly converging. The results obtained for driving sequence are shown in Figure 3-36.The vertical graph cutting lines in Figure 3-36 are showing the instances at which projection surface was changed. Vertical distortion profile is provided in Figure 3-36(a). It can be seen from the Figure 3-36(a) that after every surface change vertical geometric distortion increases but it is considerably reduced by the algorithm in next frame. For example at 4th frame vertical distortion increases from 1.8 to 4 due to surface change but at 5th frame algorithm reduced this distortion to 1. Same behavior is observable at 8th frame. Distortion reduces from 16 to 4.5 due to algorithm induced corrections. Similar behavior at 12th frame is observable, algorithm induced slight distortion at 13th frame but at very next frame distortion is reduced to 1.5. At next surface change (16th frame) distortion is 5 but algorithm reduces this distortion to 0.5. Similar adaptation is observable in horizontal distortion profile of Figure 3-36(b).

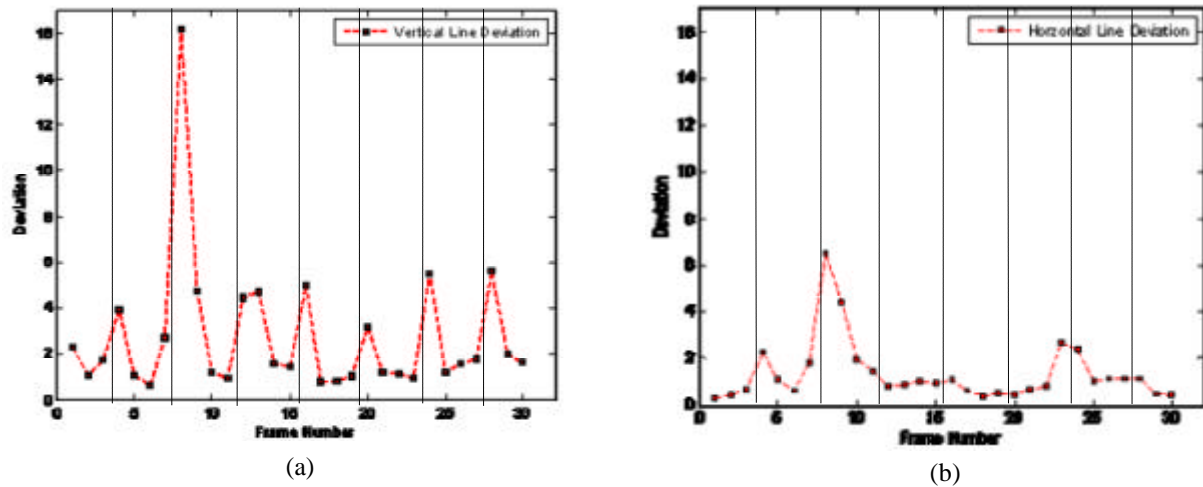(a)   (b)

Figure 3-36: Distortion profile for passive online geometric correction, fixed corner point dynamic surface (a) Vertical geometric distortion, (b) Horizontal geometric distortion

Despite of positive behavior shown by algorithm there are some frames (7th frame of Figure 3-36(a) and Figure 3-36(b), 13th frame of Figure 3-36(a) and 23rd fame of Figure 3-36(b) etc) at which algorithm induced slight distortions instead of corrections. The probable reasons of these distortions are lack of features detected or wrong feature matches. Both of these issues are related to feature detection and matching phase. Like all other feature based approaches this approach also depend upon amount of strong features present in the image.

3.5.4.3 Comparison: Passive and Hybrid Techniques for Dynamic Surfaces

The CC% values for both techniques are shown in Figure 3-37. Vertical lines are showing the instances at which surface was changed. As apparent from the data present in Figure 3-37, hybrid technique never failed on fixed corner point dynamic surface. But proposed passive approach suffers from distortion in 3rd 14th and 22nd frames. Negative values of CC% for these frames indicate that, algorithm has induced distortion in the image instead of correction. This distortion may be due to lack of features in these frames. It can be concluded from Figure 3-37 that active technique performed better than passive
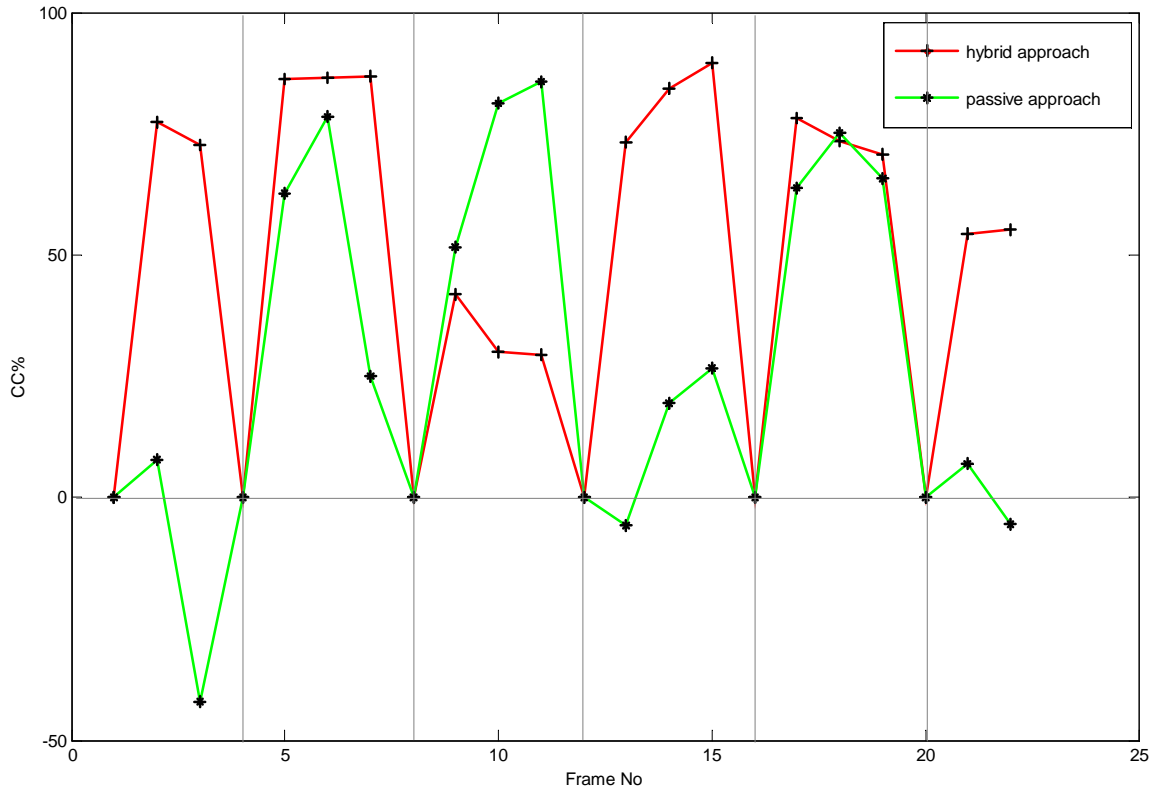
Figure 3-37: comparison of active and passive approaches for fixed corner points dynamic surfaces.

3.5.5 Comparison: Proposed Passive online Approach and Other Published Techniques

The summary of techniques surveyed is presented in Table 2-1. Among these techniques, if Yang & Welch [4] and Yamanaka [9] are computationally optimized, they may be extended to the scenarios where surfaces are dynamic but projector-camera relative positions are fixed. This is because, algorithms proposed in [4] and [9] had a fundamental constraint of fixed camera-projector relative position. Unlike [4] and [9], if passive online technique proposed in this thesis is computationally optimized and moving corner points are estimated at run time. It may be extended to the scenarios where surfaces are dynamic and projector-camera relative position is changing.

Chapter 4

CONCLUSIONS AND DISCUSSION

In this work, the aim was to check the feasibility of passive online geometric calibration techniques for quadric projection surfaces. This chapter concludes the work. Section 4.1 concludes block based methods. Section 4.2 concludes work of feature based approach. Conclusion of dynamic surfaces is given in section 4.3.

4.1 Approach 1: Block Based Methods for Quadric Surfaces

Since there are nonlinear scaling and rotations in the captured images, so block based methods in exhaustive search pattern cannot be used to perform passive online geometric calibration.

4.2 Approach 2: Feature Based Methods for Quadric Surfaces

Both hybrid and passive SIFT [29] based approaches using MLSD [11] can be used because the results of experiments are consistent and achieved acceptable geometric correction. The cumulative correction for hybrid and passive online geometric correction techniques is 40% and 30% respectively. The results suggest that, hybrid geometric correction technique is better than passive online geometric correction technique. However, passive online geometric technique is advantageous because it does not require offline display area estimation.

4.3 Dynamic Surfaces

It is apparent from achieved results that, both hybrid and passive online geometric correction techniques can be used to perform geometric correction of fixed corner point dynamic surfaces. For dynamic surface, the only constraint is fixed corner points; however display surface can be deformable.

Since the work done in this study is implemented on dynamic surfaces having fixed corner

points. Implementation of proposed passive online technique for movable corner points can be a possible extension of this work, however such implementation faces following questions.

1. How to determine if corner points of the surface have been moved.

2. Like all other feature based algorithms, proposed technique depends mainly on the number and strength of available features. Therefore a robust feature extraction algorithm is required (SIFT fails at some frames see section 3.5.4.2) which can provide reliable point based correspondence to MLSD algorithm.

If both of these points are addressed, the proposed passive online approach may be employed to perform geometric correction of dynamic surface with movable corner points.

<div align="right">**Chapter 5**</div>

<div align="center">**FUTURE WORK**</div>

Based upon findings, following future work is suggested.

1. It can be seen from the CC% plots that CC% never achieved its maximum value i.e. 100. Optimization of proposed algorithm for CC% maximization to achieve maximal geometric correction is required. One suggestion to perform such optimization is to take average of previous and current Bezier points.

2. The results shown in this work did not include any timing analysis of proposed approaches. For speed optimization, timing analysis of proposed work is required.

3. Since this work was limited to simulation environments. The results for practical environment were obtained for single frame which can be extended to real time implementation. After successful deployment for real time static quadric surfaces, check the real time implementation for fixed corner point dynamic surfaces.

4. Improvement of point based correspondence for MLSD using more robust feature extraction and matching method.

5. Hand-held projector based interactions have movable corner points and deformable display surfaces. Therefore, successful implementation for movable corner point dynamic surface will make the proposed passive online algorithm suitable for hand-held projector based applications.

REFERENCES

[1]   R. Raskar, "Projectors: Advanced Graphics and Vision Techniques," SIGGRAPH 2004 Course 22 Notes, pp. 1-166, 2004.

[2]   T. Yoshida, Y. Hirobe, H. Nii, N. Kawakami, and S. Tachi, "Twinkle: Interacting with physical surfaces using handheld projector," 2010 IEEE Virtual Reality Conference VR, IEEE, pp. 87-90, 2010.

[3]   C .Cruz-Neira, D.J. Sandin, T.A. DeFanti, R Kenyon, and J.C. Hart, "The CAVE, Audio Visual Experience Automatic Virtual Environment," Communications of the ACM, pp. 64-72, June 1992.

[4]   R. Yang, and G. Welch, "Automatic Projector Display Surface Estimation using Every-Day Imagery," in 9th International Conference in Central Europe on Computer Graphics, Visualization and Computer Vision, pp. 1-7, 2001.

[5]   M.A. Drouin, P.M. Jodoin, and J. Prémont, "Camera–Projector Matching using Unstructured Video," Machine Vision and Applications, Jul. 2011.

[6]   T. Johnson, and H. Fuchs, "Real-Time Projector Tracking on Complex Geometry using Ordinary Imagery," Proceeding of IEEE International Workshop on Projector-Camera Systems (ProCams), 2007.

[7]   H. Choi, D. Kyoung, and K. Jung, "Real-Time Image Correction," Proceeding of HCI International, pp. 345-354, 2007.

[8]   H. Park, M. Lee, B. Seo, and J. Park, "Simultaneous Geometric and Radiometric Adaptation to Dynamic Surfaces with a Mobile Projector-Camera System," IEEE Transactions on Circuits and Systems for Video Technology, vol. 18, no. 1, pp. 110-115, 2008.

[9]   T. Yamanaka, F. Sakaue, and J. Sato, "Adaptive Image Projection onto Non-planar Screen Using Projector-Camera Systems," 20th International Conference on Pattern Recognition, pp. 307-310, Aug. 2010.

[10]   M.A.Drouin, P. M. Jodoin, and J. Prémont, "Camera-Projector Matching using an Unstructured Video Stream," in IEEE Computer Society Conference on Computer Vision and Pattern Recognition Workshops (CVPRW), pp. 33–40, 2010

[11]   S. Schaefer, T. Mcphail, and J. Warren, "Image Deformation using Moving Least Squares," ACM Transactions on Graphics, vol. 2, pp. 533–540, 2003.

[12]   Atif, Rehan, Mutahir, and Haris, "DICMS Technical Report," 2009

[13]   L. A. Piegl, and W. Tiller, "The NURBS Book," 2nd ed. Berlin: Springer Verlag, pp. 25-78, 1997

[14]   R. Raskar, and P. Beardsley, "iLamps: Geometrically Aware and Self-Configuring Projectors," in ACM SIGGRAPH 2003 Conference Proceedings, pp. 1-10, 2003.

[15]   J. L. Posdamer, and M. D. Altschuler, "Surface Measurement by Space-Encoded Projected Beam Systems," Computer Graphics and Image Processing 18 (1982), no. 1, ISSN 0146-664X, pp. 1–17, 1982.

[16]   D. Caspi, N. Kiryati, S. Member, and J. Shamir, "Range Imaging with Adaptive Color Structured Light," IEEE Transactions on Pattern Analysis and Machine Intelligence, vol. 20, no. 5, pp. 470-480, 1998.

[17] R. Raskar, M. S. Brown, R. Yang, W-C. Chen, G. Welch, H. Towles, B. Seales, and H. Fuchs, "Multi-Projector Displays using Camera-Based Registration," Proceedings of the Conference on Visualization, pp. 161-168, Oct 1999.

[18] Ruigang Yang, David Gotz, Justin Hensley, Herman Towles, and Michael S. Brown, "PixelFlex: A Reconfigurable Multi-Projector Display System," IEEE Visualization, ISBN 0-7803-7200-X, pp. 167–174, 2001.

[19] R. Sukthankar, R. G. Stockton, and M. D. Mullin, "Smarter Presentations? Exploiting Homography in Camera-Projector Systems," International Conference on Computer Vision, vol. 1, pp. 247-253, 2001.

[20] R. Sukthankar, and G. Wallace, "Scalable Alignment of Large-Format Multi-Projector Displays Using Camera Homography Trees," IEEE Visualization, VIS 2002, pp. 339-346, 2002.

[21] R. Raskar, G. Welch, M. Cutts, A. Lake, L. Stesin, and H. Fuchs, "The Office of the Future: A Unified Approach to Image-Based Modeling and Spatially Immersive Displays," in COMPUTER GRAPHICS Proceedings, Annual Conference Series, SIGGRAPH 98, pp. 1-10, 1998.

[22] D. Cotting, R. Ziegler, M. Gross, and H. Fuchs, "Adaptive Instant Displays: Continuously Calibrated Projections using Per-Pixel Light Control," EUROGRAPHICS 2005, vol. 24, no. 3, pp. 705–714, 2005.

[23] J. Batlle, E. Mouaddib, and J. Salvi, "Recent Progress in Coded Structured Light as a Technique to Solve the Correspondence Problem? A Survey," Pattern Recognition, vol. 31, no. 7, pp. 963-982, 1998.

[24] J. Salvi, J. Pagès, and J. Batlle, "Pattern Codification Strategies in Structured Light Systems," Pattern Recognition, vol. 37, no. 4, pp. 827-849, Apr. 2004.

[25] Y. Yasumuro, M. Imura, Y. Manabe, O. Oshiro, and K. Chihara, "Projection-Based Augmented Reality with Automated Shape Scanning," Processing of SPIE, 2005.

[26] S. Zollmann, T. Langlotz, O. Bimber, and J. Herder, "Passive-Active Geometric Calibration for View-Dependent Projections onto Arbitrary Surfaces," Journal of Virtual Reality and Broadcasting, vol. 4, no. 6, 2007.

[27] J. Zhou, L. Wang, A. Akbarzadeh, and R. Yang, "Multi-Projector Display with Continuous Self-Calibration," in Proceedings of the 5th ACM/IEEE International Workshop on Projector camera systems, vol. 1, no. 212, 2008

[28] R. Szeliski, "Image Alignment and Stitching: A Tutorial", vol. 1. 2006.

[29] D. G. Lowe, "Distinctive Image Features from Scale-Invariant Keypoints," International Journal of Computer Vision, vol. 60, no. 2, pp. 91-110, Nov. 2004.

[30] MLSD   MATLAB   Code: http://www.mathworks.com/MATLABcentral/fileexchange/12249-moving-least-squares

[31] Video Sequences used are available at: http://trace.eas.asu.edu/yuv/

[32] Pictures used for actual setup: http://www.wallpaperpictures.com/edenpics-com-pix.html.

[33] C. Harris, and M. Stephens, "A Combined Corner and Edge Detector". In Proceedings of the 4th Alvey Vision Conference, 1988, 147–151.

[34] I. E. G. Richardson, "H.264 and MPEG-4 Video Compression," West Sussex: John Wiley& Sons Ltd, 2003.

[35] NCC MATLAB code: http://www.mathworks.com/help/toolbox/images/ref/normxcorr2.html

[36]   Z. Wang, A. C. Bovik, H. R. Sheikh, and E. P. Simoncelli, "Image Quality Assessment: from Error Visibility to Structural Similarity," IEEE Transactions On Image Processing: a Publication of the IEEE Signal Processing Society, vol. 13, no. 4, pp. 1-14, Apr. 2004.

[37]   SSIM MATLAB Code: https://ece.uwaterloo.ca/~z70wang/research/ssim/ssim_index.m.

Appendix

A. BEZEIR TRANSFORMATION

This thesis revolves around a polynomial parametric transformation known as Bezier transformation [13].

The analysis of Bezier transformation is given below

$$P(u,v) \; ? \; \sum_{i?0}^{n} \sum_{j?0}^{m} B_i^n(u) B_j^m(v) K_{i,j}$$

$$P(u,v) \; ? \; \sum_{i?0}^{n} B_i^n(u) \sum_{j?0}^{m} B_j^m(v) K_{i,j}$$

Where

$$B_i^n(u) \; ? \; \begin{pmatrix} n \\ i \end{pmatrix} u^i (1 \, ? \, u)^{n?i}$$

Putting $? ? \; ??\bullet??? \; ? ? \; ?$ and using binomial theorem given as follows

$$\begin{pmatrix} n \\ i \end{pmatrix} a^i (b)^{n?i} \; ? \; (a \, ? \, b)^n$$

$$P(u,v) \; ? \; (a \, ? \, b)^n (c \, ? \, d)^m K_{i,j} \quad \begin{matrix} i \, ? \, [0,n] \\ j \, ? \, [0,m] \end{matrix}$$

Surface of order (n, m) is defined by (n+1, m+1) control points. So for 2nd order surface which is also known as quadric (3, 3) total nine control points are required. Figure A-1 shows the position of nine control points.

For purely quadric surfaces 2nd order Bezier transformation is sufficient, however if small bumps are present or surface is piecewise quadric higher order Bezier transformation should be used. Instead of higher order Bezier transformation, Bezier subdivision can also be used. According to Bezier subdivision total image is divided into sub patches. Then 2nd order Bezier transformation is applied on every sub patch. Since 2nd order Bezier transformation takes less time as compared to higher order Bezier, so the use of Bezier subdivision speeds up the process of transformation for complex surfaces.

Formula for Bezier sub patches; for n^{th} level of subdivision, an image is divided into 4^n sub patches i.e.

- 0th level of Bezier subdivision: $4^0=1$ patch,
- 1st level of Bezier subdivision: $4^1=4$ sub patches.
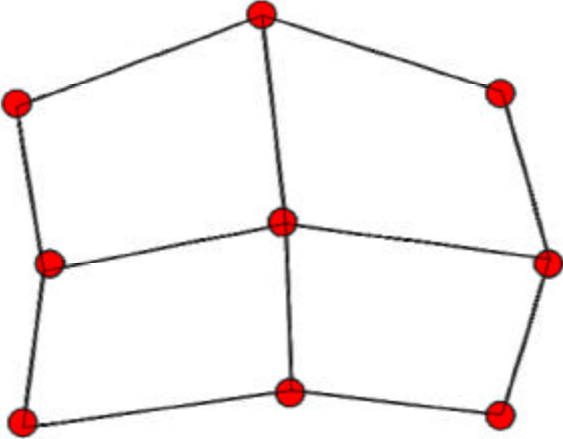- 2nd level of Bezier subdivision: $4^2=16$ sub patches.

Figure-A- 1: 0th order Bezier Control Points

The control points required for Bezier subdivision are shown in Figure A-2. Big circles (red color) show 0th level of subdivision control points. Medium circles (green color) correspond to control points required for 1st level of subdivision whereas points corresponding to small circles (blue color) are additionally required if 2nd level of subdivision is considered
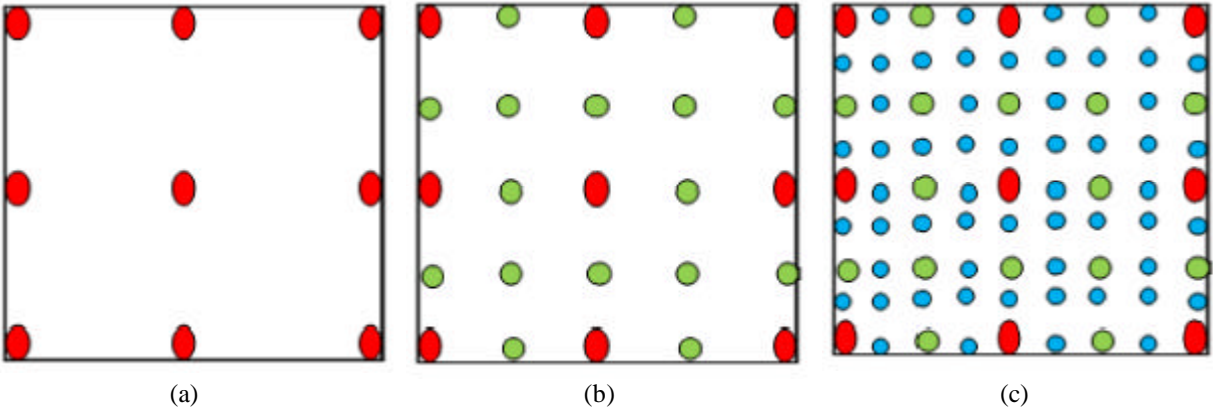

(a)   (b)   (c)

Figure-A- 2: Points required for Bezier subdivision
(a) 0th level subdivision, (b) 1st level of subdivision, (c) 3rd level of subdivision.